Université de Mons
Faculté Polytechnique – Service de Mécanique Rationnelle, Dynamique et Vibrations
31, Bld Dolez - B-7000 MONS (Belgique)
065/37 42 15 – georges.kouroussis@umons.ac.be

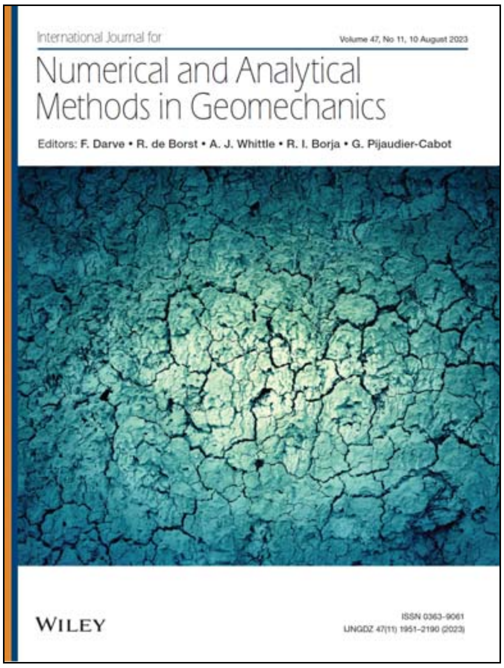

L. Qu, G. Kouroussis, J. Lian, X. Ding, Vertical dynamic interaction and group efficiency factor for floating pile group in layered soil', *International Journal for Numerical and Analytical Methods in Geomechanics*, 47 (11): 1953–1978, 2023.

Received: 3 January 2023 | Revised: 12 April 2023 | Accepted: 12 April 2023

DOI: 10.1002/nag.3546

RESEARCH ARTICLE

WILEY

Vertical dynamic interaction and group efficiency factor for floating pile group in layered soil

Liming Qu[1] | Georges Kouroussis[2] | Jing Lian[3] | Xuanming Ding[3]

[1]Faculty of Geosciences and Environmental Engineering, Southwest Jiaotong University, Chengdu, China

[2]Faculty of Engineering, Department of Theoretical Mechanics, Dynamics and Vibrations, University of Mons, Mons, Belgium

[3]College of Civil Engineering, Key Laboratory of New Technology for Construction of Cities in Mountain Area, Chongqing University, Chongqing, China

Correspondence
Liming Qu, Faculty of Geosciences and Environmental Engineering, Southwest Jiaotong University, Chengdu 610031, China.
Email: hustqlm@163.com

Jing Lian, College of Civil Engineering, Key Laboratory of New Technology for Construction of Cities in Mountain Area, Chongqing University, Chongqing, China
Email: lianjingswjtu@163.com

Funding information
National Natural Science Foundation of China, Grant/Award Number: 52208370; Applied Basic Research Programs of Science and Technology Department in Sichuan Province, China, Grant/Award Number: 2022NSFSC1086

Abstract

This paper theoretically estimates the dynamic pile–soil interaction and the group efficiency factor for pile group in layered soil through energy-based method. The vertical dynamic interaction of partially embedded single piles and their surrounding layered soil is analytically deduced from Hamilton's principle. Combined with a series of numerical simulations, the soil attenuation factor from energy method is modified for adapting to the wave speed variation in various layers. Then, the pile-to-pile interaction factor is directly solved with the help of the transfer-matrix method. The dynamic governing equation of pile group with an elevated rigid cap is established by superposing the pile-to-pile interaction factors. Finally, the dynamic impedance of pile group is obtained and derived into a group efficiency factor. Compared with the plane strain method, this present method can produce a more suitable soil attenuation factor and a dynamic interaction factor at low frequency range, which is exploited for practical engineering design. The effects of subsoil layer, subsoil layer, and unembedded pile segment on group efficiency factor are investigated. The results show that the real part of group efficiency factor decreases at high frequency range for a small pile spacing, which may be detriment to the pile group capacity. Besides that, the combined effects of unembedded segment and weak surface soil on group efficiency factor are highlighted.

KEYWORDS

dynamic interaction, group efficiency factor, layered soil, modified energy method, Pile group

1 | INTRODUCTION

Pile foundations are widely used for supporting superstructures such as bridge piers, high-rise buildings, transmission towers because of their merits of high capacity and good serviceability in various geological environments.[1–6] Estimating the dynamic performance under the loads from traffic vehicles,[7] earthquake action,[8] vibrating machine, wind, and flood is often a challenging task due to its complex frequency-dependency.[9–12] In addition to the engineering design, dynamic impedance knowledge of piles is also fundamental to the scour detection of bridges using vibration-based method.[13–17] For pile groups subjected to vertical dynamic loads, each pile interacts with the other piles through soil reaction. Rational estimations for pile–soil interaction and pile-to-pile interaction have attracted many researchers' attention.[18–21] Nowadays, four types of method have been developed to obtain both soil attenuation factor and dynamic interaction factor between adjacent piles: (a) the formulation based on Voigt model[22–24]; (b) the

 © 2023 John Wiley & Sons Ltd.

formulation from plane stain method[18,25–28]; (c) analytical methods based on continuum model[20,29,30]; (d) numerical approaches based on the finite element method (FEM), the difference method, the boundary element method or discrete element method.[21,31–35] The numerical calculation in dynamic domain often requires a cumbersome discretization treatment,[36,37] and significant running time and computer resources, which usually means high cost in engineering design. The spring and damping coefficient in Voigt models are empirical and have to be calibrated before application.[38] For layered soil, Voigt model is not convenient because a large number of experiments have to be done to obtain satisfactory coefficients for each layer. The soil attenuation factor from plane stain method is dependent with soil depth and cannot reflect the influences of pile geometric and soil stiffness variation. Besides that, plane stain method tends to overestimate the pile–soil interaction at low frequencies because it neglects the stress gradient in vertical direction.[39] According to Kanellopoulos and Gazetas,[21] inelasticity would drastically reduce the vertical interaction factors. Thus, the aforementioned overestimation may be not safe. Generally, continuum-based method can produce accurate dynamic responses of pile–soil system. Integral transformation and energy method are two types of common techniques to solve the dynamic governing equations.[28,40–45] Using continuum-based method, the dynamic impedance of single piles that are right resting on rigid rock, floating in homogeneous soil, installed in nonhomogeneous soil are accurately formulated.[46]

However, few of the existing studies compare the soil attenuation factor from continuum-based method, plane strain method and numerical method.[47] Furthermore, most of the continuum-based studies on the vertical dynamic response of pile group simplify the tip condition as end-bearing to produce a rigorous solution.[30,43] Moreover, the conventional energy-based method assumes that the soil attenuation factor is depth-independent in vertically loaded pile–soil system.[42,48–50] The feasibility of energy method for the dynamic pile-to-pile interaction in layered soil remains justified and deserves further study due to complex wave diffraction. Also, the parameter studies on variation of work efficiency against load frequency for floating pile group are far from sufficient.

The objective of this study is twofold. Firstly, a theoretical method that can amend/avoid the overestimation to dynamic pile–soil interaction from plane strain method is developed by combining variational analysis and numerical simulations. The present method accounts for the wave propagation difference in adjacent soil layers by modifying the soil attenuation factor produced from energy method. The pile-to-pile interaction factor is directly deduced in the form of an explicit matrix expression without introducing special diffraction factor due to pile rigidity or "reinforcing" effect.[18] Dynamic responses of pile group are obtained with the aid of superposing interaction factors.[51,52] Secondly, based on the calculation results, the effects of following main parameters involving layered soil profile on the group efficiency factor of floating pile group are examined: subsoil layer stiffness, stiffness and thickness of surface layer, and length of unembedded pile segment. This study can provide a possible reference to explore a continuum-based formulation for dynamic soil–structure interaction considering the effects of nonhomogeneous soil.

2 | PROBLEM DEFINITION

The problem considered here is the harmonic vibration of floating pile group partially embedded in layered soil overlying compressible or rigid rock as illustrated in Figure 1A. For solving the pile group problem in Figure 1A, two elementary problems for soil attenuation factor and pile-to-pile interaction factor are illustrated in Figure 1B,C. All the piles under the same cap have identical geometrical and mechanical properties: pile length L, circular diameter $d = 2r_\mathrm{p}$, cross-section area A_p, Young's modulus E_p, and density ρ_p. The surrounding soil has a total of N layers in which M layers are around the pile rod and the rest N-M layers are below the pile tip.

The pile is routinely treated as a linearly elastic rod and each soil layer is treated as a homogeneous, isotropic, and viscoelastic material. Since this study mainly focuses on the small-strain mechanical behavior of pile–soil system, the contact between piles and soil is assumed to be perfect without slippage or separation at pile–soil interface. The soil damping is considered as hysteretic type, that is, frequency independent. The basic properties for each ith soil layer is: Young's modulus E_si, mass density ρ_si, Poisson's ratio of υ_si, and damping ratio κ_i. In order to simplify the dynamic analysis, the complex forms of Young's modulus, shear modulus, and Lame's constant are introduced as $E^*_\mathrm{si} = E_\mathrm{si}(1 + 2\mathrm{i}\kappa_\mathrm{i})$,$G^*_\mathrm{si} = E^*_\mathrm{si}/[2(1 + \upsilon_\mathrm{si})]$, and $\lambda^*_\mathrm{si} = E^*_\mathrm{si}\upsilon_\mathrm{si}/[(1 + \upsilon_\mathrm{si})(1 - 2\upsilon_\mathrm{si})]$ respectively. The pile cap is excited by a vertical force $F(t) = F_0 e^{\mathrm{j}\omega t}$, where F_0 denotes the amplitude, ω represents the force circular frequency, t and j denote time and the imaginary unit, respectively.

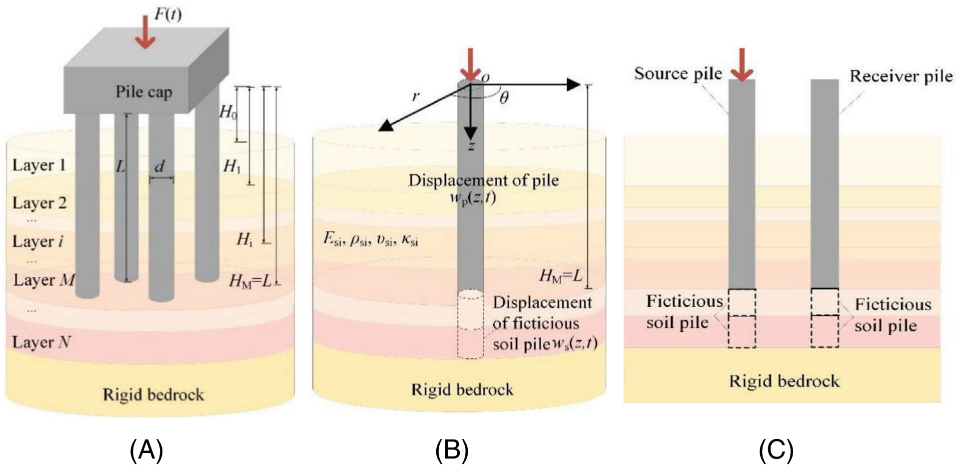

FIGURE 1 Partially embedded floating piles in layered soil. (A) Pile group. (B) Single pile model for soil attenuation factor. (C) Double-pile system for pile-to-pile interaction factor.

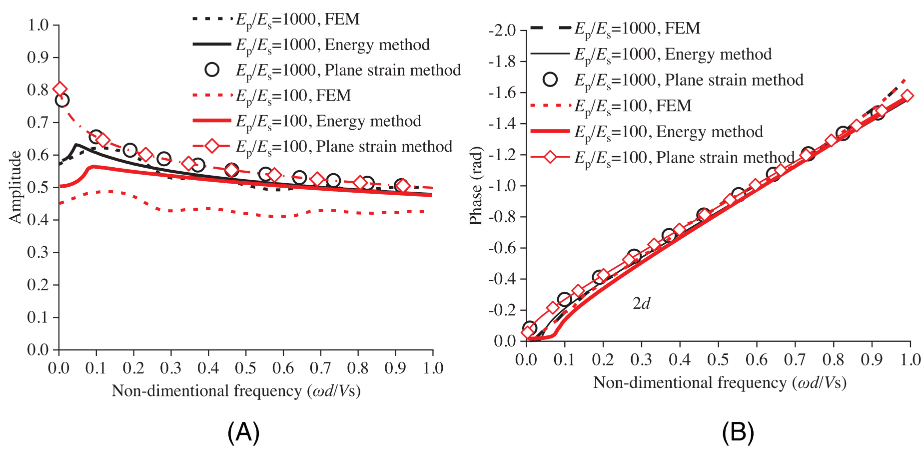

FIGURE 2 Comparisons of soil attenuation factor in homogenous soil (s = 2d). V_s varies with E_p/E_s ratio. (A) Amplitude. (B) Phase.

3 | THEORETICAL FRAMEWORK AND SOLVING PROCESS

3.1 | Vibration of single pile and its surrounding soil

3.1.1 | Displacement model and energy function for pile–soil system

Solving the dynamic impedance of single pile and corresponding soil attenuation factor is essential for the responses of pile group. As shown in Figure 1B, the soil column beneath the pile tip is modeled by a fictitious soil pile to establish a continuum-based model. The radial displacement in the fictitious soil pile is neglected. For the situation of vertical vibration, the previous studies[40,42] have concluded that the radial displacement and circumferential displacement of a pile–soil system play a trivial role in its vertical responses and are neglected in this study. The displacement pattern on the pile cross section is assumed to be uniform and thus the pile becomes one-dimensional shaft. Because no soil resistance acts on the unembedded pile segment, it can be inferred that the pile–soil interaction is exclusively determined by the embedded segment. Previous studies[20,46,53] have confirmed that the soil displacement $w_s(r, z, t)$ can be expressed as the product of two individual functions: $w(z, t)$ and $\phi(r)$:

$$w_s(r, z, t) = w(z, t)\phi(r) \tag{1}$$

where $w(z,t)$ denotes the axial displacement of embedded pile shaft $w_{\mathrm{p}}(z,t)$ when $H_0 \le z \le L$; and $w(z,t)$ denotes the vertical displacement of the fictitious soil pile $w_{\mathrm{s}}(z,t)$ when $L < z \le H_{\mathrm{N}}$, which is given by:

$$w(z,t)=\begin{cases} w_{\mathrm{p}}(z,t), (H_0 \le z \le L) \\ w_{\mathrm{s}}(z,t), (z > L) \end{cases} \tag{2}$$

The function $\phi(r)$ of radial coordinate r in Equation (1) is a dimensionless value that represents the attenuation factor of soil displacement with respect to the axial displacement $w_{\mathrm{p}}(z,t)$ of the loaded pile shaft. Naturally, $\phi(r)$has following boundary condition:

$$\phi(r) = \begin{cases} 1, 0 \le r \le r_{\mathrm{p}} \\ 0, r \to \infty \end{cases} \tag{3}$$

For a vibrating pile–soil system, the total energy ($\mathfrak{R}$) should include three types of components: the kinetic energy T, the potential energy U, and the external work W. The integral forms of those energy components in all soil layers and the pile shaft (including the fictitious one) can be given by the following:

$$\begin{aligned} T &= T_{\mathrm{unembeddedpile}} + T_{\mathrm{embeddedpile}} + T_{\mathrm{soil}} \\ &= \int_0^{H_0} \frac{1}{2}\rho_{\mathrm{p}} A_{\mathrm{p}} \left(\frac{\partial w_{\mathrm{pi}}}{\partial t}\right)^2 dz + \sum_{i=1}^{M} \left[\int_{H_{\mathrm{i-1}}}^{H_{\mathrm{i}}} \frac{1}{2}\rho_{\mathrm{p}} A_{\mathrm{p}} \left(\frac{\partial w_{\mathrm{pi}}}{\partial t}\right)^2 dz + \int_{H_{\mathrm{i-1}}}^{H_{\mathrm{i}}} \int_0^{2\pi} \int_{r_{\mathrm{p}}}^{\infty} \frac{1}{2}\rho_{\mathrm{si}} \phi^2 \left(\frac{\partial w_{\mathrm{pi}}}{\partial t}\right)^2 r dr d\theta \mathrm{d}z \right] \\ &+ \sum_{j=\mathrm{M}+1}^{N} \left[\int_{H_{\mathrm{j-1}}}^{H_{\mathrm{j}}} \frac{1}{2}\rho_{\mathrm{sj}} A_{\mathrm{p}} \left(\frac{\partial w_{\mathrm{sj}}}{\partial t}\right)^2 dz + \int_{H_{\mathrm{j-1}}}^{H_{\mathrm{j}}} \int_0^{2\pi} \int_{r_{\mathrm{p}}}^{\infty} \frac{1}{2}\rho_{\mathrm{sj}} \phi^2 \left(\frac{\partial w_{\mathrm{sj}}}{\partial t}\right)^2 r dr d\theta \mathrm{d}z \right] \end{aligned} \tag{4}$$

where H_0 is the length of unembedded pile segment and H_i is the depth of the ith soil layer (subscripts i and j indicate each layer for displacement $w_{\mathrm{p}i}$ and $w_{\mathrm{s}j}$).

$$\begin{aligned} \mathrm{U} &= U_{\mathrm{unembeddedpile}} + U_{\mathrm{embeddedpile}} + U_{\mathrm{soil}} \\ &= \int_0^{H_0} \frac{1}{2} E_{\mathrm{p}} A_{\mathrm{p}} \left(\frac{\partial w_{\mathrm{pi}}}{\partial z}\right)^2 dz + \sum_{i=1}^{M} \left[\int_{H_{\mathrm{i-1}}}^{H_{\mathrm{i}}} \frac{1}{2} E_{\mathrm{p}} A_{\mathrm{p}} \left(\frac{\partial w_{\mathrm{pi}}}{\partial z}\right)^2 dz + \int_{H_{\mathrm{i-1}}}^{H_{\mathrm{i}}} \int_0^{2\pi} \int_{r_{\mathrm{p}}}^{\infty} \frac{1}{2} \left((\lambda_s^* + 2G_s^*) \phi^2 \left(\frac{\partial w_{\mathrm{pi}}}{\partial z}\right)^2 + G_{\mathrm{s}}^* w_{\mathrm{pi}}^2 \left(\frac{\partial \phi(r)}{\partial r}\right)^2 \right) r dr d\theta dz \right] \\ &+ \sum_{j=M+1}^{N} \left[\int_{H_{\mathrm{j-1}}}^{H_{\mathrm{j}}} \frac{1}{2} (\lambda_s^* + 2G_s^*) A \left(\frac{\partial w_{\mathrm{si}}}{\partial z}\right)^2 dz + \int_{H_{\mathrm{j-1}}}^{H_{\mathrm{j}}} \int_0^{2\pi} \int_0^{\infty} \frac{1}{2} \left((\lambda_s^* + 2G_s^*) \left(\phi \frac{\partial w_{\mathrm{si}}}{\partial z}\right)^2 + G_{\mathrm{s}}^* w_{\mathrm{si}}^2 \left(\frac{\partial \phi(r)}{\partial r}\right)^2 \right) r dr d\theta dz \right] \end{aligned} \tag{5}$$

$$W = \int_{t_1}^{t_2} F(t) w(z,t)|_{z=0}\, dt \tag{6}$$

Based on the principle of least action in continuum, a mechanical system approaches its equilibrium status when the variation of the energy function $\mathfrak{R}$ during the period from t_1 to t_2 reaches its minimal value, which yields:

$$\delta\mathfrak{R} = \int_{t_1}^{t_2} (\delta T - \delta U + \delta W) dt = 0 \tag{7}$$

where $\delta(*)$ denotes the variational operator.

Substituting Equation (4), Equation (5), Equation (6) into Equation (7) and then applying the hormonic vibration condition $w(z,t) = w(z)e^{i\omega t}$ produces the following equation:

$$
\begin{aligned}
\delta\mathfrak{R} = & \int_{t_1}^{t_2}\int_{0}^{H_0} \frac{1}{2}\rho_p A_p \left(\frac{\partial w_{pi}}{\partial t}\right)^2 dzdt + \int_{t_1}^{t_2}\int_{0}^{H_0} \frac{1}{2}E_p A_p \left(\frac{\partial w_{pi}}{\partial z}\right)^2 dzdt \\
& + \sum_{i=1}^{M}\left\{\omega^2\rho_p A_p \int_{t_1}^{t_2}\int_{H_{i-1}}^{H_i} w_p\delta w_p dtdz + 2\pi\rho_s\omega^2 \int_{t_1}^{t_2}\int_{H_{i-1}}^{H_i}\int_{r_p}^{\infty} \phi^2 w_p\delta w_p rdrdzdt + 2\pi\rho_s\omega^2 \int_{t_1}^{t_2}\int_{H_{i-1}}^{H_i}\int_{r_p}^{\infty} r\phi w_p^2\delta\phi drdzdt\right\} \\
& + \sum_{i=1}^{M}\left\{-E_p A_p \int_{t_1}^{t_2}\left(\frac{\partial w_p}{\partial z}\delta w_p\Big|_{H_{i-1}}^{H_i} - \int_{H_{i-1}}^{H_i}\frac{\partial^2 w_p}{\partial z^2}\delta w_p dz\right)dt - \pi\left(\lambda_{si}^* + 2G_{si}^*\right)\int_{t_1}^{t_2}\right. \\
& \times\left[2\int_{r_p}^{\infty}\left(\frac{\partial w_p}{\partial z}\right)\phi^2 r\delta w_p\Big|_{H_{i-1}}^{H_i} - 2\int_{0}^{L}\int_{r_p}^{\infty} r\phi^2\left(\frac{\partial^2 w_p}{\partial z^2}\right)\delta w_p drdz + 2\int_{0}^{L}\int_{r_p}^{\infty}\phi\left(\frac{\partial w_p}{\partial z}\right)^2\delta\phi rdrdz\right]dt \\
& + \sum_{j=M+1}^{N}\left\{\omega^2\rho_s A_p \int_{t_1}^{t_2}\int_{L}^{\infty} w_s\delta w_s dtdz + 2\pi\, rho_s\omega^2 \int_{t_1}^{t_2}\int_{H_{j-1}}^{H_j}\int_{r_p}^{\infty} r\phi^2 w_s\delta w_s drdzdt + 2\pi\rho_s\omega^2 \int_{t_1}^{t_2}\int_{H_{j-1}}^{H_j}\int_{r_p}^{\infty} r\phi w_s^2\delta\phi drdzdt\right\} \\
& + \sum_{j=M+1}^{N}\left\{-\left(\lambda_s^* + 2G_s^*\right)A_p \int_{t_1}^{t_2}\left(\frac{\partial w_s}{\partial z}\delta w_s\Big|_{H_{j-1}}^{H_j} - \int_{0}^{L}\frac{\partial^2 w_s}{\partial z^2}\delta w_s dz\right)dt - \pi\left(\lambda_{sj}^* + 2G_{sj}^*\right)\right. \\
& \times\int_{t_1}^{t_2}\left[2\int_{r_p}^{\infty}\left(\frac{\partial w_s}{\partial z}\right)\phi^2 r\delta w_s\Big|_{H_{j-1}}^{H_j} - 2\int_{r_p}^{\infty}\int_{L}^{\infty} r\phi^2\left(\frac{\partial^2 w_s}{\partial z^2}\right)\delta w_s dzdr + 2\int_{H_{j-1}}^{H_j}\int_{r_p}^{\infty} r\phi\left(\frac{\partial w_s}{\partial z}\right)^2\delta\phi drdz\right]dt \\
& -\pi G_s^*\int_{t_1}^{t_2}\left[2\int_{H_{j-1}}^{H_j}\int_{r_p}^{\infty}\left(\frac{\partial\phi}{\partial r}\right)^2 w_p r\delta w_p drdz + 2\int_{H_{j-1}}^{H_j} w_p^2\frac{\partial\phi}{\partial r} r\delta\phi dz\Big|_{r_p}^{\infty} - 2\int_{H_{j-1}}^{H_j}\int_{r_p}^{\infty} w_p^2\left(r\frac{\partial^2\phi}{\partial r^2} + \frac{\partial\phi}{\partial r}\right)\delta\phi drdz\right]dt\Bigg\} \\
& -\pi G_s^*\int_{t_1}^{t_2}\left[2\int_{H_{j-1}}^{H_j} w_s^2\left(\frac{\partial\phi}{\partial z}\right) r\delta\phi dz\Big|_{r_p}^{\infty} - 2\int_{r_p}^{\infty}\int_{H_{j-1}}^{H_j} w_s^2\left(r\frac{\partial^2\phi}{\partial r^2} + \frac{\partial\phi}{\partial z}\right)\delta\phi dzdr + 2\int_{H_{j-1}}^{H_j}\int_{r_p}^{\infty} w_s\left(\frac{\partial\phi}{\partial r}\right)^2\delta w_s rdrdz\right]dt\Bigg\} \\
= & \ 0
\end{aligned}
\tag{8}
$$

3.1.2 | Pile response

Simplifying Equation (8) yields the following form:

$$
f_0(w_{p0})\delta w_{p0} + \sum_{i=1}^{M} f_i(w_{pi})\delta w_{pi} + \sum_{j=M+1}^{N} f_j(w_{sj})\delta w_{sj} + g(\phi)\delta\phi = 0 \tag{9}
$$

Since δw_{p0}, δw_{pi},δw_{sj}, and $\delta\phi$ are basically independent functions with each other, the prerequisite for Equation (9) is that the corresponding four coefficients f_0, f_{i}, f_{j},and g before the variation functions should always equal zero at any condition. Therefore, the dynamic governing equations of the unembedded pile segment, embedded segment, and the fictitious soil pile can be respectively expressed as:

$$f_0 = E_{\mathrm{p}}A\frac{\partial^2 w_{\mathrm{p0}}}{\partial z^2} + \rho_{\mathrm{p}}A\omega^2 w_{\mathrm{p0}}= 0{,}0 \le z < H_0 \tag{10a}$$

$$f_{\mathrm{i}} = \left(E_{\mathrm{p}}A{+}2t_{\mathrm{i}}\right)\frac{\partial^2 w_{\mathrm{pi}}}{\partial z^2} - \left[k_{\mathrm{i}} - (\alpha_{\mathrm{i}} + \rho_{\mathrm{p}}A)\omega^2\right] w_{\mathrm{pi}}= 0{,}1 \le i \le M \tag{10b}$$

$$f_{\mathrm{j}} = \left[\left(\lambda_{\mathrm{sj}}^* + 2G_{\mathrm{sj}}^*\right)A{+}2t_{\mathrm{j}}\right]\frac{\partial^2 w_{\mathrm{sj}}}{\partial z^2} - \left[k_{\mathrm{j}} - (\alpha_{\mathrm{j}} + \rho_{\mathrm{sj}}A)\omega^2\right] w_{\mathrm{sj}}= 0{,}M < j \le N \tag{10c}$$

For the sake of simplicity, the terms of $\lambda_{\mathrm{sj}}^* + 2G_{\mathrm{sj}}^*(M < j \le N)$ in Equation (10c), E_{p} in Equation (10a) and Equation (10b) are expressed in the form of equivalent elastic modulus $\overline{E_{\mathrm{i}}}(0 \le i \le N)$, which is given by:

$$\overline{E_{\mathrm{i}}}=\begin{cases} E_{\mathrm{p}}, (0 \le i \le M) \\ \lambda_{\mathrm{si}}^* + 2G_{\mathrm{si}}^*, (M < i \le N) \end{cases} \tag{11}$$

After employing similar transformations to k_{i},k_{j}, α_{i}, α_{j}, ρ_{p}, and ρ_{sj}, along with letting $w_{\mathrm{pi}} = w_{\mathrm{sj}}, (M < i \le N, j = i)$, Equations (10a–10c) have the following unified expression:

$$\left(\overline{E_i}A{+}2t_i\right)\frac{\partial^2 w_{\mathrm{pi}}}{\partial z^2} - \left[k_i - (\alpha_i + \rho_i A)\omega^2\right] w_{\mathrm{pi}}= 0{,}0 \le i \le N \tag{12}$$

where $k_i = \alpha_i = t_i = 0$ when i= 0, and it has the following expressions when $0 < i \le N$:

$$t_i{=}\pi\left(\lambda_{\mathrm{si}}^* + 2G_{\mathrm{si}}^*\right)\int_{r_{\mathrm{p}}}^{\infty}\phi^2 r dr \tag{13a}$$

$$\alpha_i{=}\ 2\pi\rho_{\mathrm{si}}\int_{r_{\mathrm{p}}}^{\infty}\phi^2 r dr \tag{13b}$$

$$k_i{=}\ 2\pi G_{\mathrm{si}}^*\int_{r_{\mathrm{p}}}^{\infty}\left(\frac{\partial\phi}{\partial r}\right)^2 r dr \tag{13c}$$

The general solution of Equation (12) is given by:

$$w_{\mathrm{pi}}(z) = B_i e^{\lambda_{\mathrm{i}} z} + C_i e^{-\lambda_i z}, (0 \le i \le N) \tag{14}$$

where

$$\lambda_{\mathrm{i}} = \sqrt{\frac{k_i - (\alpha_i + \rho_i A)\omega^2}{\overline{E_i}A + 2t_i}} \tag{15}$$

The axial force $Q_{\mathrm{i}}(z)$ in pile shaft in the ith layer is given by:

$$Q_i(z) = -\left(\overline{E_i}A + 2t_i\right)\frac{\partial w_i}{\partial z} = -B_i\zeta_i e^{\lambda_i z} + C_i\zeta_i e^{-\lambda_i z} \tag{16}$$

where

$$\zeta_i{=}\sqrt{[k_i - (\alpha_i + \rho_i A)\omega^2]\left(\overline{E_i}A + 2t_i\right)} \tag{17}$$

The axial displacement and force between any two adjacent layers should be identical. Consequently, the recurrence relation for pile displacement and force between the top and bottom of ith layer can be deduced in matrix form as the following:

$$\begin{bmatrix} w_{\mathrm{pi}}(H_{\mathrm{i+1}}) \\ Q_{\mathrm{pi}}(H_{\mathrm{i+1}}) \end{bmatrix} = [t]_{\mathrm{i}} \begin{bmatrix} w_{\mathrm{pi}}(H_{\mathrm{i}}) \\ Q_{\mathrm{pi}}(H_{\mathrm{i}}) \end{bmatrix} \tag{18}$$

where it has:

$$[t]_{\mathrm{i}} = \begin{bmatrix} \cosh(\lambda_{\mathrm{i}}\Delta H_{\mathrm{i}}) & -\frac{1}{\lambda_{\mathrm{i}}\left(\overline{E_{\mathrm{i}}}A+2t_{\mathrm{i}}\right)}\sinh(\lambda_{\mathrm{i}}\Delta H_{\mathrm{i}}) \\ -\lambda_{\mathrm{i}}\left(\overline{E_{\mathrm{i}}}A+2t_{\mathrm{i}}\right)\sinh(\lambda_{\mathrm{i}}\Delta H_{\mathrm{i}}) & \cosh(\lambda_{\mathrm{i}}\Delta H_{\mathrm{i}}) \end{bmatrix} \tag{19}$$

Hence the responses relationship between the pile top and the bottom of layer N (the final layer) can be obtained by applying the matrix transfer method, which yields:

$$\begin{bmatrix} w_{\mathrm{p}}(H_{\mathrm{N}}) \\ Q_{\mathrm{p}}(H_{\mathrm{N}}) \end{bmatrix} = \begin{bmatrix} T_{11}^{1} & T_{12}^{1} \\ T_{21}^{1} & T_{22}^{1} \end{bmatrix} \begin{bmatrix} w_{\mathrm{p}}(0) \\ Q_{\mathrm{p}}(0) \end{bmatrix} = \left[T^{1}\right] \begin{bmatrix} w_{\mathrm{p}}(0) \\ Q_{\mathrm{p}}(0) \end{bmatrix} \tag{20}$$

where

$$\left[T^{1}\right] = \left[t^{1}\right]_{\mathrm{N}}\left[t^{1}\right]_{\mathrm{N-1}}\cdots\left[t^{1}\right]_{2}\left[t^{1}\right]_{1}\left[t^{1}\right]_{0} \tag{21}$$

Substituting the boundary condition of zero vertical soil displacement on the rigid rock at $z = H_{\mathrm{N}}$ yields the following:

$$w_{\mathrm{p}}(H_{\mathrm{N}}) = T_{11}^{1}w_{\mathrm{p}}(0) + T_{12}^{1}Q_{\mathrm{p}}(0) = 0 \tag{22}$$

Thus the dynamic axial impedance of the partially embedded pile can be written as:

$$K_{\mathrm{d}}(0) = \frac{Q_{\mathrm{p}}(0)}{w_{\mathrm{p}}(0)} = -\frac{T_{11}^{1}}{T_{12}^{1}} \tag{23}$$

3.1.3 | Soil vibration and attenuation function $\phi(r)$

Collecting the coefficients of $\delta\phi$ from Equation (8) produces the following equation:

$$g(\phi) = \frac{\partial^2\phi}{\partial r^2} + \frac{1}{r}\frac{\partial\phi}{\partial r} - \psi^2\phi = 0 \tag{24}$$

where

$$\psi = \sqrt{\frac{n_{\mathrm{s1}} - n_{\mathrm{s2}}\omega^2}{m_{\mathrm{s}}}} \tag{25}$$

$$m_{\mathrm{s}} = \sum_{i=1}^{N}\int_{H_{i-1}}^{H_i} 2\pi G_{\mathrm{s}i}^{*} w_{\mathrm{p}i}^{2} dz \tag{26a}$$

$$n_{\mathrm{s1}} = \sum_{i=1}^{N}\int_{H_{i--1}}^{H_i} 2\pi\left(\lambda_{\mathrm{s}i}^{*} + 2G_{\mathrm{s}i}^{*}\right)\left(\frac{\partial w_{\mathrm{pi}}}{\partial z}\right)^{2} dz \tag{26b}$$

$$n_{\mathrm{s2}} = \sum_{i=1}^{N}\int_{H_{i-1}}^{H_i} 2\pi\rho_{\mathrm{s}i} w_{\mathrm{p}i}^{2}\mathrm{d}z \tag{26c}$$

Solving Equation (24) and substituting the boundary conditions in Equation (3) will give the general solution of $\phi(r)$ as following:

$$\phi(r) = \frac{\mathrm{K}_0(\psi r)}{\mathrm{K}_0(\psi r_\mathrm{p})} \tag{27}$$

where $\mathrm{K}_0(*)$ is the modified Bessel function of the second kind of zero order.

3.1.4 | Solution technique

The pile displacement at any given depth z can be finally expressed by the soil parametersk_i,t_i,α_i, which rely on the displacement decay function ϕ. It is clear that ϕ is determined by other soil parameters m_s, $n_{\mathrm{s}1}$, $n_{\mathrm{s}2}$ and ψ from Equation (25) to Equation (27). An iterative procedure[42] is thus applied to obtain the expected results. First, an initial empirical value of around 1.0 is made for the parameter ψ to calculate the decay function ϕ through Equation (27). Then the undetermined coefficients k_i,t_i,α_i, and λ_i can be instantly calculated through Equations (13a)–(13c) and Equation (15). The pile displacement subsequently can be obtained through Equation (19) and Equation (23). Recalculating the parameters of m_s, $n_{\mathrm{s}1}$, $n_{\mathrm{s}2}$ through Equations (26a-c), the value of ψ can be updated by Equation (33). Repeating the entire process until the tolerance between the new and old value of $\psi$is less than 10^{-3}. Finally, the dynamic impedance of partially embedded single piles can be calculated through Equation (23).

3.2 | Dynamic interaction between adjacent piles

As shown in Figure 1C, pile 1# is loaded by a vertical harmonical excitation while pile 2# does not carry any load. In such a double pile system, pile 1# is called the source pile and pile 2# is called the receiver pile. It is assumed that the origin of coordinate locates on the top of loaded pile (pile 1#) and the radial distance of pile 1# from pile 2# is denoted by s. The secondary effects of the receiver pile to the source pile are neglected in this study. Thus the vibration of ith segment for a receiver pile (including the fictitious soil pile) obeys the following governing equation:

$$\left(\overline{E_i}A{+}2t_i\right)\frac{\partial^2 w_{21,i}}{\partial z^2} + \rho_i A\omega^2 w_{21,i} - \left(k_i - \alpha_i\omega^2\right)\left(w_{21,i}{-}\overline{w_i}\right) = 0, 0 \le i \le N \tag{28}$$

where $\overline{w_i}$ is the frequency-domain soil displacement of free field in the absence of receiver pile. Note that $\overline{w_i}$ equals to zero when $i = 0$ for the unembedded pile segment. For the depth $z \ge H_0$ or $i \ge 1$, soil displacement $\overline{w_\mathrm{i}}$ is given by:

$$\overline{w_i} = \phi_i(s)w_{\mathrm{p}i}(z) = \phi_i(s)\left(B_i e^{\lambda_i z} + C_i e^{-\lambda_i z}\right), (1 \le i \le N) \tag{29}$$

The solution of Equation (28) can be expressed as:

$$w_{21i} = \frac{k_\mathrm{i} - \alpha_i\omega^2}{2\lambda_i\left(\overline{E_i}A{+}2t_i\right)}\phi_i(s)z\left(-B_i e^{\lambda_i z} + C_i e^{-\lambda_i z}\right) + D_i e^{\lambda_i z} + F_i e^{-\lambda_i z} \tag{30}$$

Then the axial force can be written as:

$$\begin{aligned} Q_{21i}(z) &= -\left(\overline{E_i}A + 2t_i\right)\frac{\partial w_{21i}}{\partial z} \\ &= -\frac{k_i - \alpha_i\omega^2}{2\lambda_i}\phi_i(s)\left[\frac{Q_i(z)}{\zeta_i} - z\lambda_i w_i(z)\right] - \lambda_i D_i\left(\overline{E_i}A + 2t_i\right)e^{\lambda_i z} + \lambda_i F_i\left(\overline{E_i}A + 2t_i\right)e^{-\lambda_i z} \end{aligned} \tag{31}$$

Combining Equations (14), (16), (30), and (31), the unknown coefficients D_i and F_i can be expressed as the function of $w_i(z)$, $Q_i(z)$,w_{21i}, and Q_{21i} as following:

$$D_i = \frac{1}{2\lambda_i\left(\overline{E}_i A + 2t_i\right)}\left[\frac{1}{e^{\lambda_i z}}\lambda_i\left(\overline{E}_i A + 2t_i\right)w_{21i} - \frac{Q_{21i}(z)}{e^{\lambda_i z}} - \frac{k_i - \alpha_i\omega^2}{2\zeta_i e^{\lambda_i z}}\phi_i(s)\left(z + \frac{1}{\lambda_i}\right)Q_i(z) + z\frac{k_i - \alpha_i\omega^2}{2e^{\lambda_i z}}\phi_i(s)w_i(z)\right] \tag{32a}$$

$$F_i = \frac{1}{2\left(\overline{E}_i A + 2t_i\right)\lambda}\left[w_{21i}e^{\lambda_i z}\left(\overline{E}_i A + 2t_i\right)\lambda + Q_{21i}(z)e^{\lambda_i z} - \frac{k_i - \alpha_i\omega^2}{2\lambda_i}\phi_i(s)z\lambda_i w_i(z)e^{\lambda_i z} + \left(\frac{k_i - \alpha_i\omega^2}{2\lambda_i}\right)\phi_i(s)\left\{\frac{1}{\zeta_i} - \lambda_i z\frac{1}{\zeta_i}\right\}Q_i(z)e^{\lambda_i z}\right] \tag{32b}$$

Thus the recurrence relation for displacement and force between the top and bottom of the ith layer receiver pile segment can be deduced in matrix form as the following:

$$\begin{bmatrix} w_{21i}(H_{i+1}) \\ Q_{21}(H_{i+1}) \end{bmatrix} = \left[t^1\right]_i \begin{bmatrix} w_{21i}(H_i) \\ Q_{21}(H_i) \end{bmatrix} + \left[t^2\right]_i \begin{bmatrix} w_i(H_i) \\ Q_i(H_i) \end{bmatrix} \tag{33}$$

where $[t^1]_{\mathrm{i}}$ can refer to Equation (19), and matrix $[t^2]_{\mathrm{i}}$is given by:

$$\left[t^2\right]_i = \begin{bmatrix} -\Delta H_i \dfrac{k_i - \alpha_i\omega^2}{2\lambda_i\left(\overline{E}_i A + 2t_i\right)}\phi_i(s)\sinh(\lambda_i\Delta H_i) & \dfrac{k_i - \alpha_i\omega^2}{2\lambda_i\zeta_i\left(\overline{E}_i A + 2t_i\right)}\phi_i(s)\left[-\dfrac{1}{\lambda}\sinh(\lambda_i\Delta H_i) + \Delta H_i\cosh(\lambda_i\Delta H_i)\right] \\ \dfrac{k_i - \alpha_i\omega^2}{2\lambda_i}\phi_i(s)\{\sinh(\lambda_i\Delta H_i) + \lambda_i\Delta H_i\cosh(\lambda_i\Delta H_i)\} & -\dfrac{k_i - \alpha_i\omega^2}{2\zeta_i}\Delta H_i\phi_i(s)\sinh(\lambda_i\Delta H_i) \end{bmatrix} \tag{34}$$

Considering the compatibility of stress and deformation at the interface of adjacent layers, the responses relationship between the pile top and the bottom of layer N (the final soil layer) are given by:

$$\begin{bmatrix} w_{21}(L) \\ Q_{21}(L) \end{bmatrix} = \left[T^1\right] \begin{bmatrix} w_{21}(0) \\ Q_{21}(0) \end{bmatrix} + \left[T^2\right] \begin{bmatrix} w(0) \\ Q(0) \end{bmatrix} \tag{35}$$

where matrix $[T^1]$ can refer to Equation (21) and matrix $[T^2]$ can be calculated as:

$$\left[T^2\right] = \sum_{\mathrm{j=1}}^{\mathrm{N}} \left[t^1\right]_{\mathrm{N}}\left[t^1\right]_{\mathrm{N-1}} \cdots \left[t^1\right]_{\mathrm{j+1}}\left[t^2\right]_{\mathrm{j}}\left[t^1\right]_{\mathrm{j-1}} \cdots \left[t^1\right]_1\left[t^1\right]_0 \tag{36}$$

The vertical soil displacement $w_{21}(L)$ must be zero, which is given by:

$$w_{21}(L) = T^1_{11}w_{21\mathrm{i}}(0) + T^1_{12}Q_{21}(0) + T^2_{11}w_{\mathrm{i}}(0) + T^2_{12}Q_{\mathrm{i}}(0) = 0 \tag{37}$$

The force at the top of passive pile is zero:

$$Q_1(0) = 0 \tag{38}$$

The force at the top of active pile is written as:

$$Q_{\mathrm{i}}(0) = w_{\mathrm{i}}(0)K_{\mathrm{d}}(0) \tag{39}$$

Substituting Equations (38) and (39) into Equation (37) yields the dynamic interaction factor as following:

$$\chi_{21} = \frac{w_{21}(0)}{w(0)} = -\frac{\left(T^2_{11} + T^2_{12}K_{\mathrm{d}}(0)\right)}{T^1_{11}} \tag{40}$$

3.3 | Dynamic impedance of pile group

The method of superimposing dynamic pile-to-pile interaction factors has been proved to be efficient for solving the pile group responses in small strain range.[21,51] The equilibrium equations for a group of m piles that are connected by a no-mass

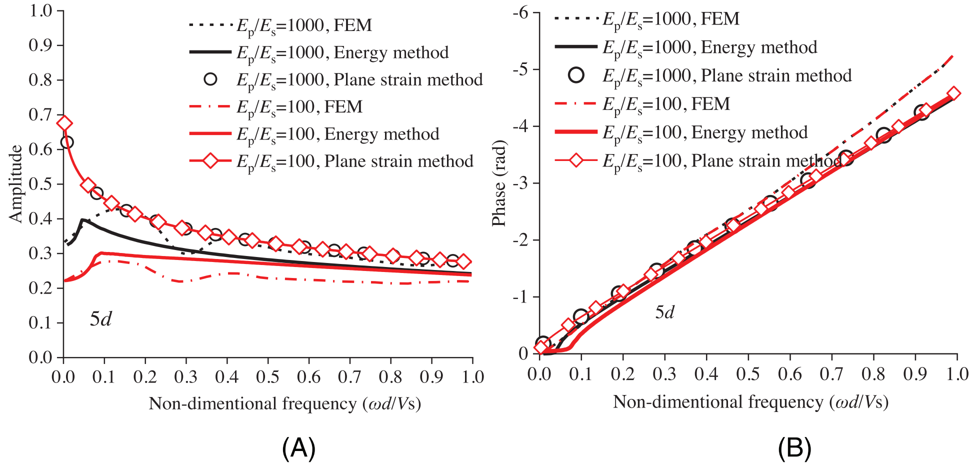

FIGURE 3 Comparisons of soil attenuation factor in homogenous soil ($s = 5d$). V_s varies with E_p/E_s ratio. (A) Amplitude. (B) Phase.

rigid cap are written as:

$$\begin{bmatrix} 0 & 1 & 1 & \cdots & 1 \\ -1 & \beta_{11} & \beta_{12} & \cdots & \beta_{1m} \\ -1 & \beta_{21} & \beta_{22} & \cdots & \beta_{2m} \\ \cdots & \cdots & \cdots & \cdots & \cdots \\ -1 & \beta_{m1} & \beta_{m2} & \cdots & \beta_{mm} \end{bmatrix} \begin{Bmatrix} u_G \dfrac{E_p A_p}{L} \\ P_1 \\ P_2 \\ \cdots \\ P_m \end{Bmatrix} = \begin{Bmatrix} P_G \\ 0 \\ 0 \\ \cdots \\ 0 \end{Bmatrix} \tag{41}$$

where u_G is the vertical displacement of the cap; P_i denote the load vertically applied on the head of ith pile and P_G is the resultant force acting on the cap; the coefficient β_{ij} can be calculated as following:

$$\beta_{ij} = \frac{E_p A_p}{k_d^j L} \chi_{ij} \tag{42}$$

The dynamic impedance for a group of square piles is therefore expressed by:

$$k_G = \frac{P_G}{u_G} \tag{43}$$

4 | VALIDATION AND COMPARISON FOR PILES IN HOMOGENOUS SOIL

4.1 | Soil attenuation factor

Figures 2 and 3 compare the soil attenuation factors for a single floating pile in a homogeneous half space obtained by three types of method: presented energy method, finite element method (FEM), and plane strain method. Basic properties of pile-soil system are unified as: $H_0 = 0$; $L = 20$ m, $r_p = 0.5$ m, $\rho_p = 2188$ kg/m^3, $E_p = 25$ GPa; $\rho_s = 1750$ kg/m^3, $E_s = 25$ GPa, $\upsilon_s = 0.49$, $\varkappa = 0.05$; Note that FEM data are obtained from the linear-elastic results in Kanellopoulos and Gazetas.[21] Presented method yields soil attenuation factor from Equation (26). The plane strain method refers Gazetas and Makris[22] and is calculated by:

$$\phi(s) = \frac{H_0^2(\omega r / V_s)}{H_0^2(\omega r_0 / V_s)} \tag{44}$$

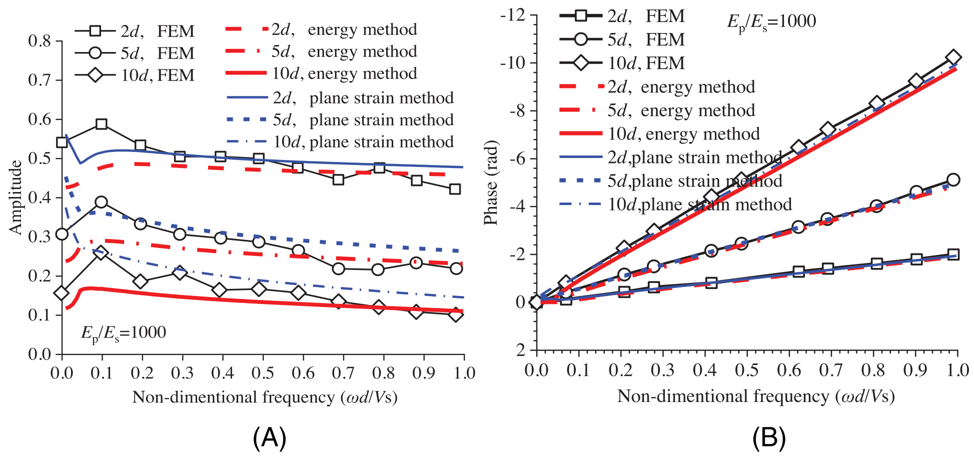

FIGURE 4 Comparisons of dynamic interaction factor in homogenous soil ($E_p/E_s = 1000$). (A) Amplitude. (B) Phase.

where s is pile spacing; $H_0^2(*)$ is the Hankel function of the second kind of zero order and V_s is the shear wave velocity in soil. In the analysis, the non-dimensional frequency a_0 is routinely used by normalizing true frequency ω by $\omega d/V$s. When $s = 2d$, Figure 2A shows that the amplitude of soil attenuation factor ϕ at $E_p/E_s = 1000$ from FEM results is around 0.57 for a static condition. As frequency increases from zero, the amplitude starts to increase to a peak value and then gradually decreases in the given frequency range. The results from energy method are very close with that from FEM at $E_p/E_s = 1000$. By contrast, plane strain method overestimates the soil attenuation factor in low frequency range and gives a relationship of continuous fall with increasing frequency. Besides that, both FEM and energy methods predict the phenomenon that amplitude of ϕ becomes smaller as soil becomes stiffer. By contrast, plane strain method could not consider the effects of E_p/E_s on vibration attenuation of surround soil. Generally, the differences of the results between the energy method and FEM are within acceptable accuracy in the geotechnical design even when the soil is relatively hard, for example, $E_p/E_s =$ 100 in Figure 2A. The phase results in Figure 2B have no significant difference, which indicates that all the three methods are competent to capture the phase features of oscillating pile–soil system. In addition, Figure 2B reflects that the phase information of the waves in surrounding soil is insusceptible to the soil stiffness for a floating pile in homogeneous soil.

When s = 5d, Figure 3A shows that energy method agrees well with the FEM in the low frequency range of $a_0 < 0.1$ for E_p/E_s = 100 and 1000. As a_0 continues to increase and exceeds the cut-off frequency, the amplitude results from FEM method decreases in fluctuation while that from energy method steadily decreases. Thus, a small result deviation between the energy method and FEM takes place. The amplitude of ϕ at $E_p/E_s = 1000$ from FEM is around 0.32 for a static condition when s = 5d, which indicates an attenuation of around 45% compared to that from FEM method when s = 2d. However, that attenuation is no more than 15% if calculated by plane strain method. The evident overestimation for soil attenuation in plane strain model demonstrates that vertical gradient of soil stress plays a significant role in low frequency range. It is also interesting to observe that the three types of methods tend to yield closer amplitude results among one another as frequency becomes higher. In Figure 3B, it is shown that the phases from FEM are slightly larger than that from both energy and plane strain methods. That is, due to the different damping effects for the Rayleigh model in FEM and hysteretic damping model.[24]

4.2 | Dynamic interaction factor

Figures 4 and 5 depict the variation of pile-to-pile interaction factor χ against frequency in the forms of amplitude and phase. Both pile and soil parameters are the same with those in Section 4.1. Figure 4A clearly shows that dynamic interaction becomes weaker as pile spacing gets farther from $s = 2d$ to $s = 10d$. Compared with the results from FEM, both energy and plane strain methods provide satisfactory prediction of interaction factor at the frequency range of $a_0 > 0.2$ when $E_p/E_s = 1000$. At the low frequency range, plane strain method produces slightly more accurate results compared with that energy method for $s = 2d$. That is a joint result of two folds. Firstly, the assumption of one-dimensional shaft for passive piles leads to a natural limitation: dynamic interaction factor is underestimated without taking pile geometry into account when the passive pile is very close to active pile. Secondly, soil attenuation factor is overestimated in plane

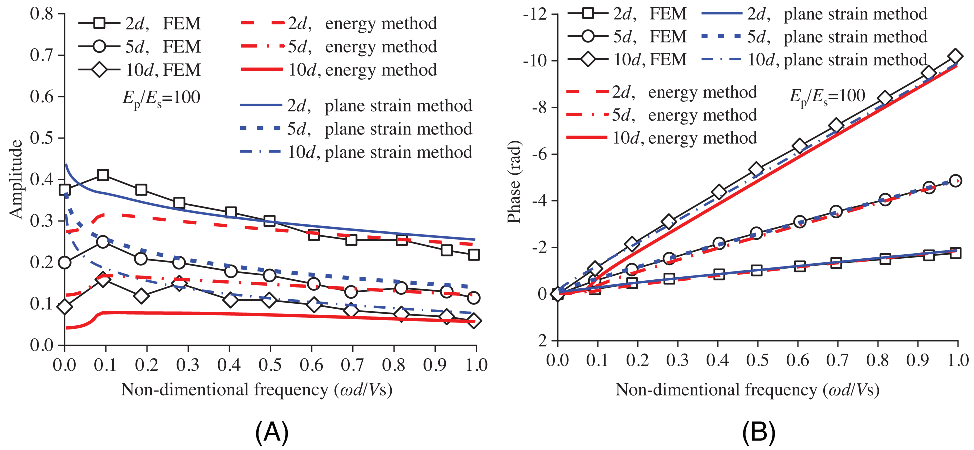

FIGURE 5 Comparisons of dynamic interaction factor in homogenous soil ($E_p/E_s = 100$). (A) Amplitude. (B) Phase.

strain method, which just provides a compensation for the above-mentioned limitation. Not surprisingly, the deviation of the plane strain method becomes more evident as the passive pile moves further from active pile, especially for the static condition. On the contrary, the deviation between energy method and FEM becomes much smaller as pile spacing s increases for the static condition. At the same time, the phases in Figure 4B from three types of methods agree very well with one another, which again confirms the efficiency of present method.

In Figure 5A, it can be estimated that the amplitude of dynamic interaction factor from FEM generally reduces by around 25%–50% in the given frequency range when the modulus ratio of E_p/E_s decreases from 1000 to 100. For the energy and plane strain methods, such reduction is around 30%–55% and 15%–50%, respectively. Basically, energy method tends to impair pile to pile dynamic interaction to some extent while plane strain method tends to strengthen dynamic interaction. From the engineering perspective, a mild impair to dynamic interaction is acceptable (if not anticipated) considering the following two facts: linearly elastic status is just an extreme case when the external force and soil strain are adequately small; amplitude of dynamic interaction factor will be suppressed a lot when non-linearity occurs.[21]

5 | COMPARISON AND MODIFICATION FOR PILES IN LAYERED SOIL

5.1 | Soil attenuation factor

In this section, a two-dimensional (2D) model that is symmetric in respect to pile axis is built to investigate the wave propagation in double-layered pile-soil system through finite element (FE) software Abaqus as shown in Figure 6. The material assumption and interface settings are the same with those in Section 2. The pile properties are: mass density ρ_p 2750 kg/m^3; Young's modulus E_p 25 GPa, Poisson's ratio 0.1, diameter $d = 1.0$ m, shaft length $L = 20d$; unembedded segment length $H_0 = 0$; soil properties for the first soil layer and the second layer are: mass density $\rho_{s1} = 1760$ kg/m^3 and $\rho_{s2} = 2200$ kg/m^3, Young's modulus $E_{s1} = 25$ MPa and $E_{s2} = 125$ MPa, damping ratio $\kappa_1 = 0.1$ and $\kappa_2 = 0.05$, Poisson's ratio $\upsilon_{s1} = \upsilon_{s2} = 0.4$. The bottom boundary of soil domain is completely fixed. Infinite elements are introduced to absorb the wave energy from the reflection of lateral boundary.[54,55] Rayleigh damping is used to account for material damping effects in viscoelastic soil domain, which is a typical simplification done by many researchers, although its limitation is in modeling realistically the energy dissipation due to material damage. Finite element meshing of soil and pile are finely done to meet the practical rule that the largest element size is not larger than one tenth of the interest wavelength.[21] The first two inherent displacement modes for the pile–soil system in double layer ground on vertical vibration are computed by the linear perturbation algorithm in Abaqus, which are transformed into 3D contour maps shown in Figure 7. Subsequently, the two coefficients α and β in Rayleigh damping can be obtained with the first two inherent frequencies ω_1 and ω_2 of pile–soil system by $\alpha = 2\kappa\omega_1\omega_2/(\omega_1+\omega_2)$ and $\beta = 2\kappa/(\omega_1+\omega_2)$. For comparisons, extra two models of single pile in homogenous soil are established by replacing the properties of double soil layers with those of solely soil layer 1 and solely soil layer 2, respectively.

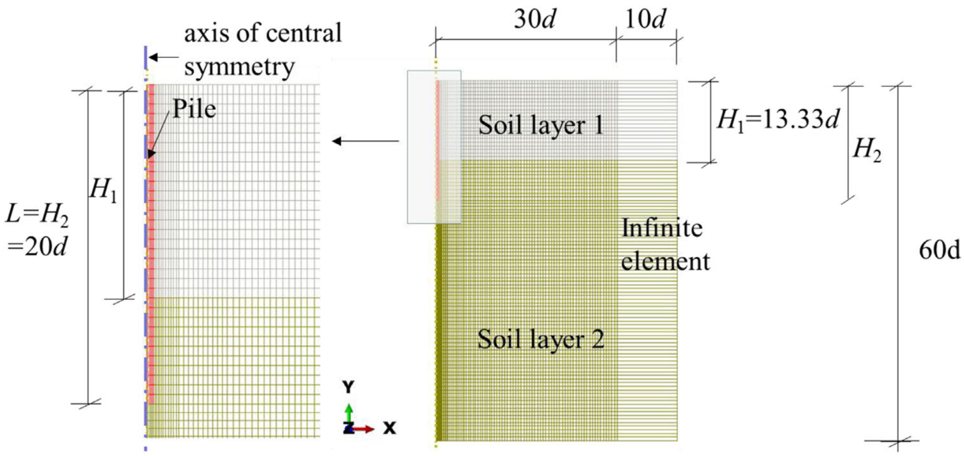

FIGURE 6 Geometrics and mesh discretization of the two-dimensional (2D) model for layered soil ($E_p/E_{s1} = 1000$; $V_{s1}/V_{s2} = 0.5$; $\rho_p/\rho_{s2} = 1.25$; $\rho_{s1}/\rho_{s2} = 0.8$; $H_1{:}L = 2{:}3$).

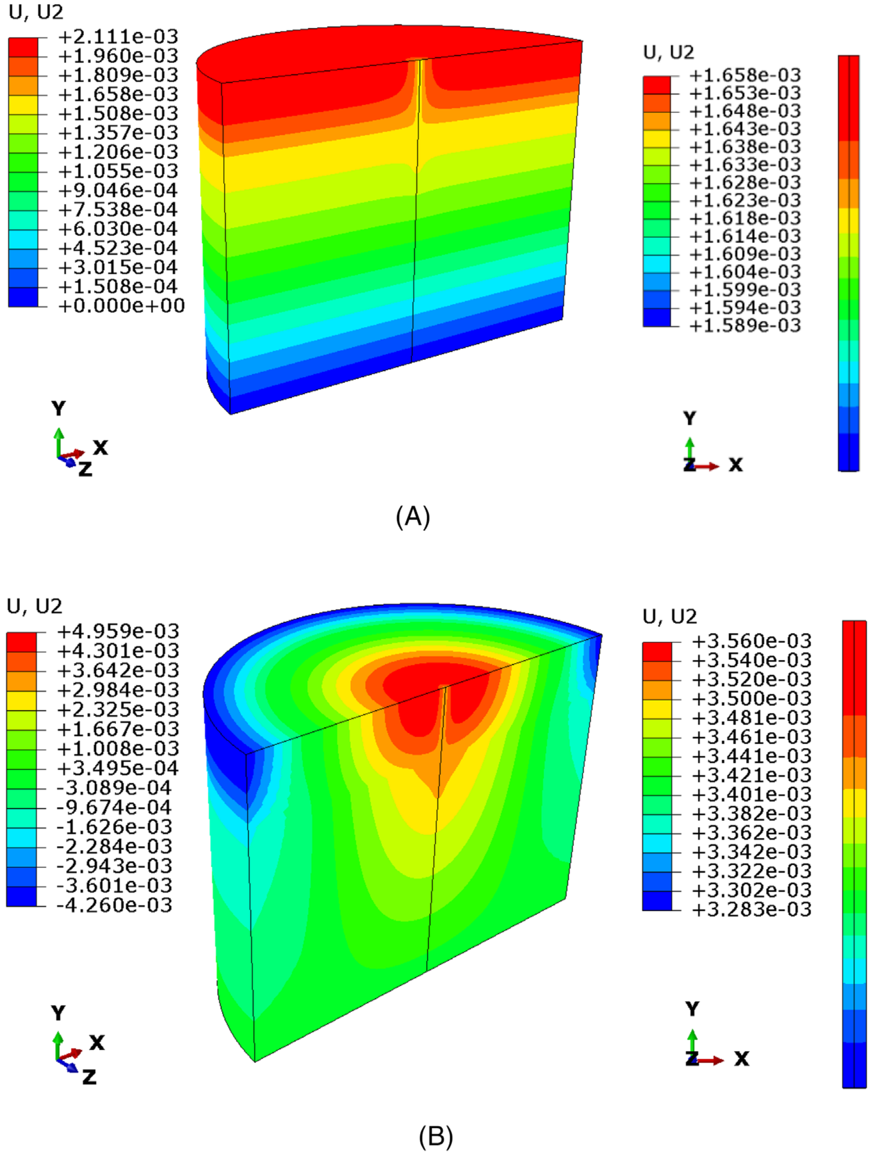

FIGURE 7 The first two inherent modes of pile–soil system in double-layered ground. (A) The first inherent mode ($\omega_1 = 9.28$ rad/s). (B) The second inherent mode ($\omega_2 = 13.96$ rad/s).

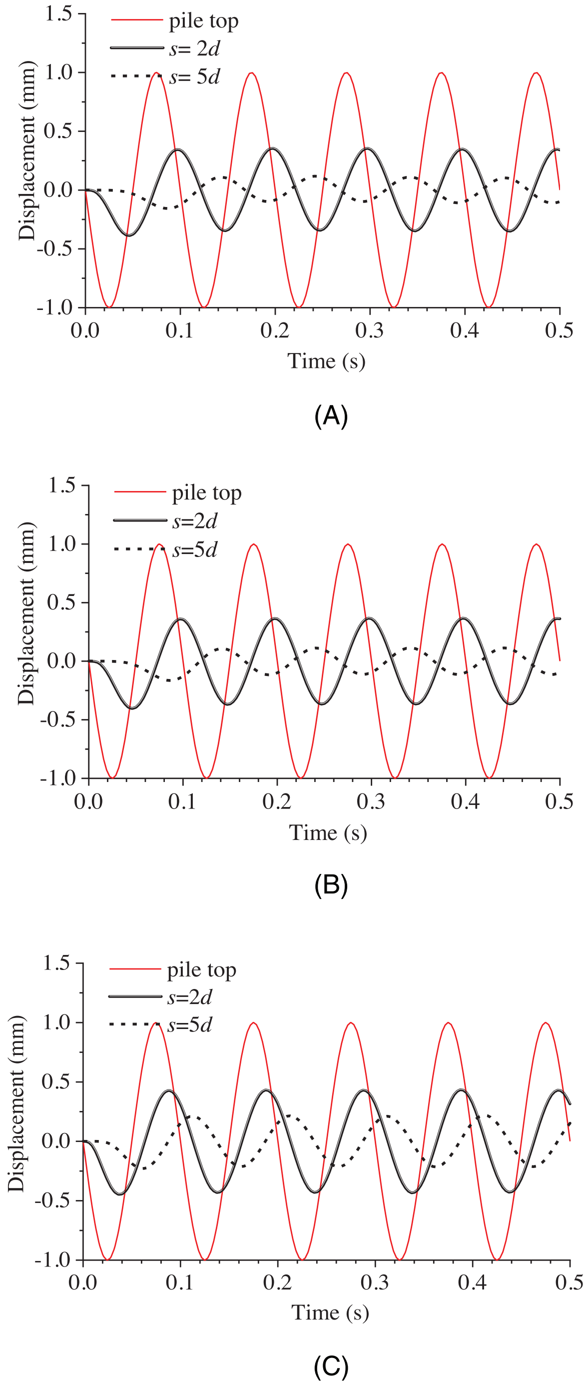

FIGURE 8 Time-domain displacements at ground level of pile–soil system with different soil profiles on harmonic excitation with frequency 10 Hz. (A) Layered soil. (B) Homogenous soil layer 1. (C) Homogenous soil layer 2.

A series of vertical harmonic excitations with various frequencies are then applied on the pile top in the form of displacement boundary. Implicit solver with iterative algorithm is employed to calculate the responses of pile–soil system on each excitation. Figure 8 shows the displacement histories of pile top and ground surface in two-layered soil and homogeneous soil models. Obvious time delays between the peak responses of pile and soil are observed in those displacement histories from Figure 8A to Figure 8C. It is also shown that the time delay of ground vibration in layered soil ($E_{s1} = 25$ MPa, $E_{s2} = 125$ MPa) is similar with that in homogenous soil layer 1 ($E_s = 25$ MPa) and is greater than those in homogenous soil layer 2 ($E_s = 125$ MPa).

Based on the time-domain displacement histories of pile and interest soil positions, the amplitude and phase of soil attenuation factor can be easily interpreted. Figure 9 compares the soil attenuation factors obtained by FEM and the energy

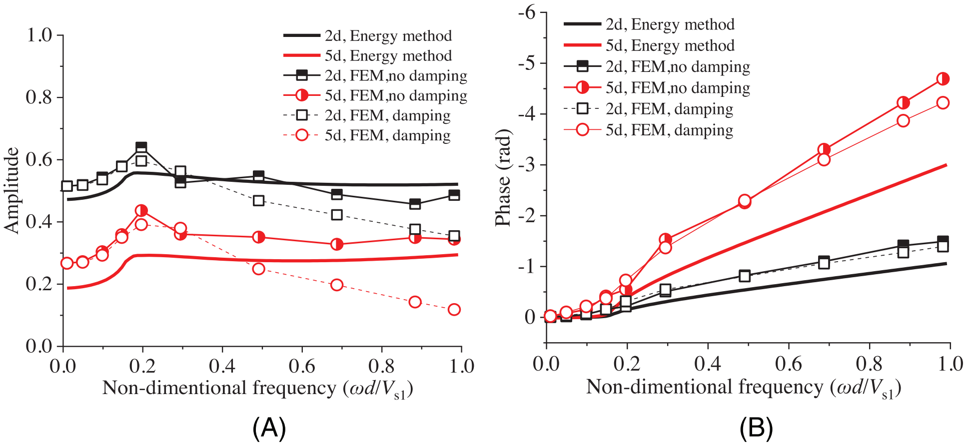

FIGURE 9 Comparisons of soil attenuation factor produced by FEM and energy method in layered soil profile. $E_{s2}/E_{s1} = 5$; $E_p/E_{s1} = 1000$. (A) Amplitude. (B) Phase.

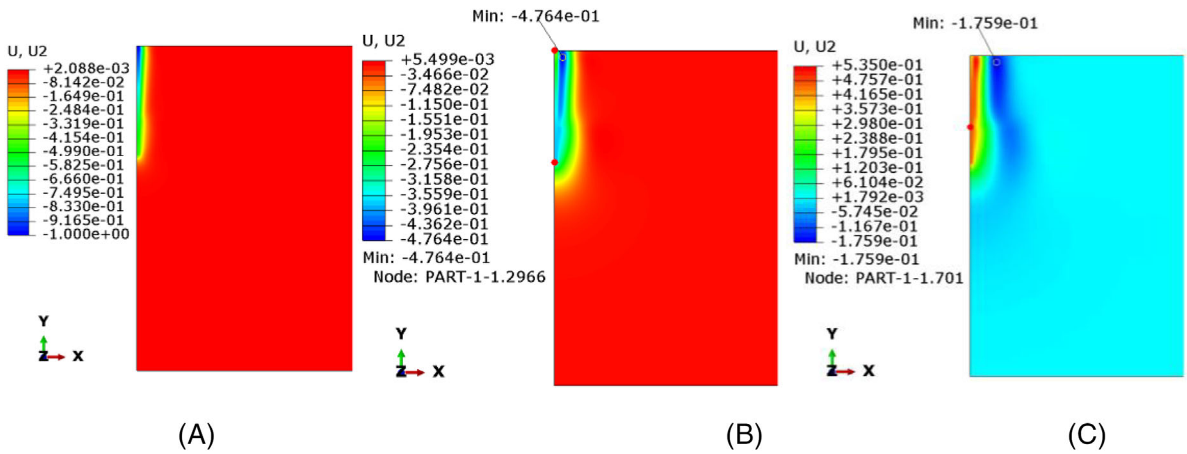

FIGURE 10 Displacement [m] contours for single pile in two-layered soil at various points of time ($f = 10$ Hz). (A) $t = 0.0025$ s, (B) $t = 0.0047$ s, (C) $t = 0.0094$ s.

method through Equation (27) in layered soil. In Figure 9A, it is shown that both those two methods predict one cut-off frequency around $a_0 = 0.2$. Before the cut-off frequency, the soil attenuation factor from FEM in the absence of soil damping obtains the similar amplitude to that in the presence of soil damping. As a_0 continues to increase, the effects of soil damping gradually become significant. Consequently, the results from FEM with damping effects prominently decrease with increasing frequency. Besides that, it appears that the amplitude results from energy method (Equation (27)) have evident difference with that from FEM with damping especially for the high frequency range. Figure 9B shows that the phase results from FEM are generally greater than those from energy method, which indicates a larger wave propagation speed through Equation (27). Also note that the effects of soil damping on the phase are much weaker than that on the amplitude. Basically, the energy method assumes that the soil attenuation factor keeps invariable along depth, which brings an artificial constraint for the wave field. In homogenous ground, that assumption would not cause significant error. In layered ground, however, the wave velocity difference between soil layers leads to non-negligible phase lags, which amplifies the prediction errors of energy method.

Figures 10–12 plot the evolution of displacement contours for the piles installed in various soil profiles with damping and subjected to a harmonic excitation of 10 Hz. At $t = 0.0025$ s when pile displacement comes to its peak, the soil displacement is rather limited shown in Figure 10A. Subsequently at $t = 0.0047$ s when the displacement at soil position $s = 2d$ has its peak, the wave front is clearly divided into two segments: the upper one is approximately parallel to pile axis, and the lower one looks like an arch in Figure 10B. That two-segment division is clearer in Figure 10C at $t = 0.0094$ s when the

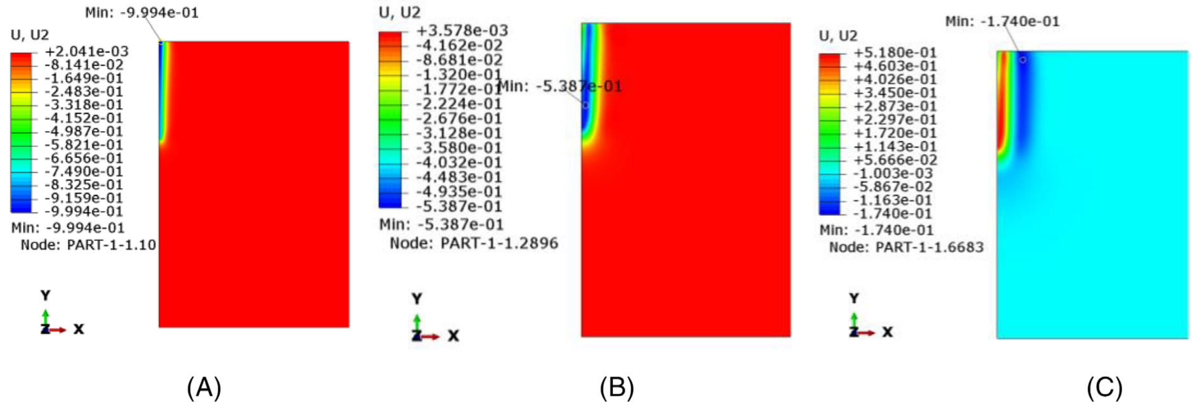

FIGURE 11 Displacement [m] contours for single pile in homogenous soil layer 1 at various points of time ($f = 10$ Hz). (A) $t = 0.0025$ s, (B) $t = 0.0047$ s, (C) $t = 0.0097$ s.

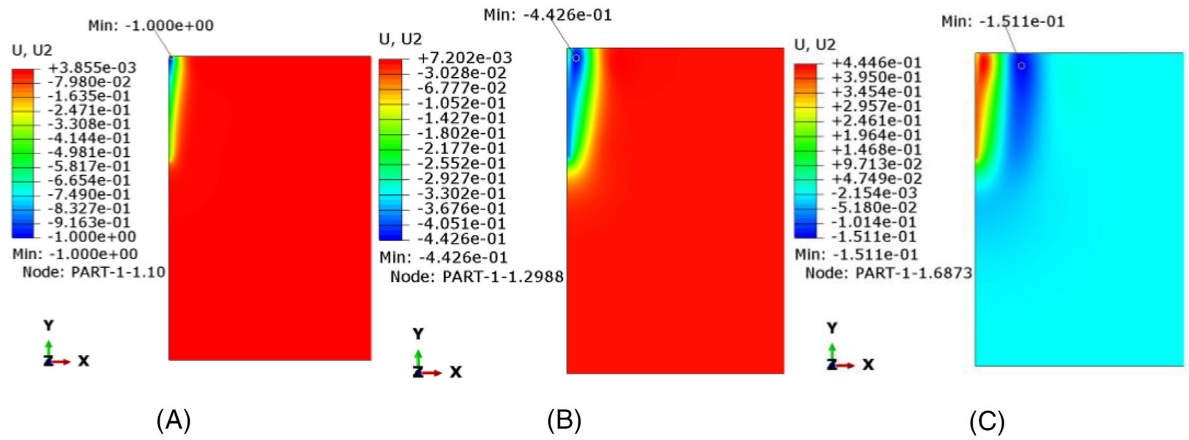

FIGURE 12 Displacement [m] contours for single pile in homogenous soil layer 2 at various points of time ($f = 10$ Hz). (A) $t = 0.0025$ s, (B) $t = 0.0046$ s, (C) $t = 0.0095$ s.

response at soil position $s = 5$d comes its peak. By the contrast, the wave fronts of displacement contours for homogeneous soil shown in Figures 11 and 12 do not show any turn point or have the feature of two-segment division.

According to the above analysis, the energy method in Section 3.1 should be modified to capture more details on the wave propagation in layered soil. We assume that the depth variation of soil attenuation factor in each homogenous layer is negligible. It means each soil layer has solely one same soil attenuation factor. An approximate method is then proposed to obtain the soil attenuation factors in different soil layers based on the idea of equivalent substitution. For the surrounding soil that has N layers, the soil attenuation factor in ith layer (ϕ_i) can be approached by that in homogenous soil with its properties equals the ith layer. In other words, the soil properties of other N-1 layers are replaced with the ith layer to calculate ϕ_i. Figures 13 and 14 depict the comparisons of soil attenuation factors at various depths in actual layered soil and hypothetical homogeneous soil through FEM for $s = 2$d and $s = 5$d, respectively. It is shown in Figure 13 that both the amplitude and phase of the soil attenuation factor from the hypothetical homogeneous soil agree quite well with those in layered soil at $H = 0$ m and $s = 2d$. At the depth of $H = 13.33$ m or the top of second layer, the approximate method predicts slightly larger amplitudes than those in layered soil shown in Figure 13A. This reflects that the soil attenuation in the second layer, to some extent, is influenced by the first layer due to the continuity conditions of displacement and stress on the interface between adjacent soil layers. Nevertheless, the phase results from approximate method are close to those in layered soil and the overall deviation for amplitude is not significant even if $E_{s2}/E_{s1} = 5$ in Figure 13. Similar results are observed in Figure 14 for $s = 5$d. Above analysis confirms that the proposed approximate method can produce satisfactory results for soil attenuation factor in layered soil.

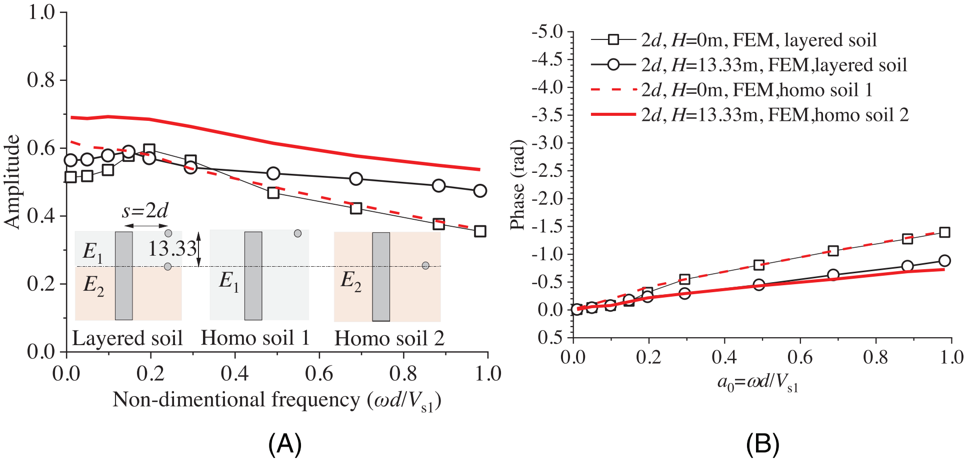

FIGURE 13 Comparisons of soil attenuation factor (s = 2d). (A) Amplitude. (B) Phase.

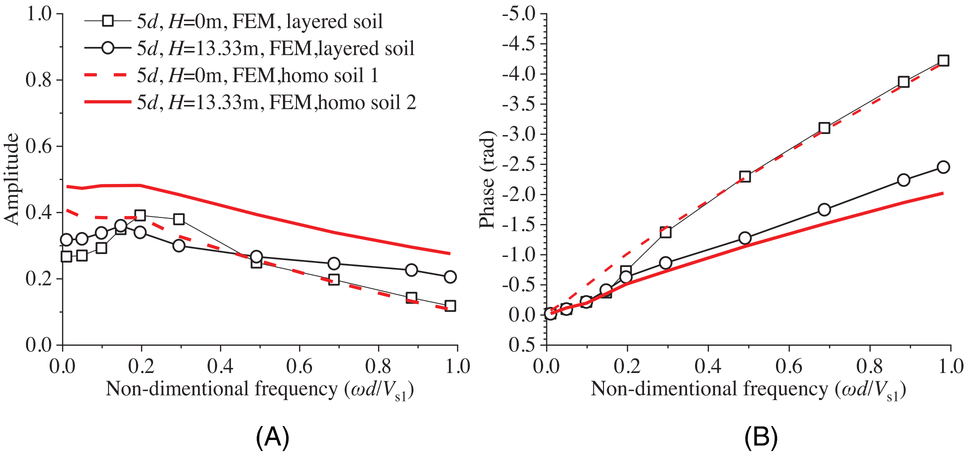

FIGURE 14 Comparisons of soil attenuation factor (s = 5d). (A) Amplitude. (B) Phase.

FIGURE 15 Geometrics and mesh discretization of the three-dimensional (3D) model for layered soil ($E_p/E_{s1} = 1000$; $V_{s1}/V_{s2} = 0.5$; $\rho_p/\rho_{s2} = 1.25$; $\rho_{s1}/\rho_{s2} = 0.8$; $H_1/L = 2/3$).

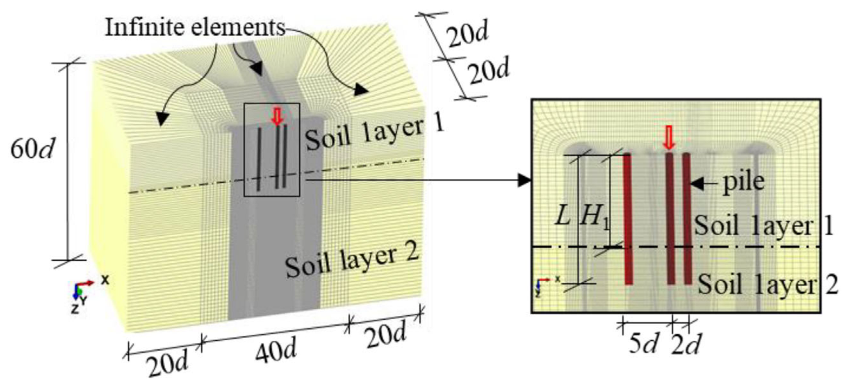

5.2 | Dynamic interaction factor

In the presence of adjacent piles, the whole of piles–soil system is non-axisymmetric. Therefore, a three-dimensional (3D) model is required to compute the dynamic pile to pile interaction factor as shown in Figure 15. The basic properties for pile and soil are same with those in Section 4.1. The adjacent passive piles locate the positions off 2d and 5d from the axis of loaded pile, respectively. C3D8 type elements are used for pile and soil, and a layer of infinite elements is employed on their periphery. Other settings on load, boundary, damping, and algorithm remains same with the 2D FE

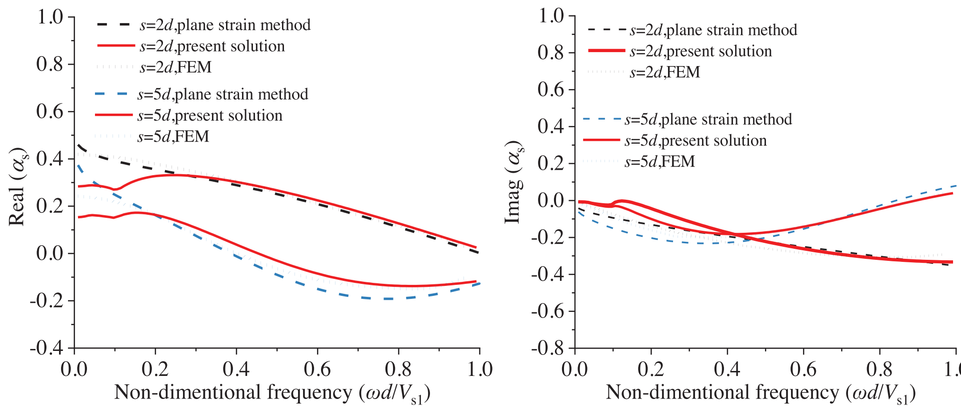

FIGURE 16 Comparisons of dynamic interaction factor from the present method, plane strain method, and FEM. (A) Real part. (B) Imaginary part.

model in Section 4.1. Figure 16 compares the real and imaginary results of dynamic interaction factor obtained from present method, plane strain method (Refer to Mylonakis and Gazetas[18]), and 3D FEM. It is observed in both Figure 16A,B that those three methods give very close results for the dynamic interaction factor when $a_0 > 0.4$. At low frequency range, the present method gives slightly smaller dynamic interaction factor than that from FEM at both s = 2d and s = 5d as shown in Figure 16A. Such underestimation mainly results from the omission of radial displacement in soil domain in the theoretical framework of energy method (refer to Salgado et al.[50]). Besides that, compared with the quick decrease of the real part when $a_0 < 0.4$ indicated by plane strain method, the variation of real part against frequency obtained by FEM and the present method are milder.

6 | RESULTS ANALYSIS AND PARAMETER STUDY ON GROUP EFFICIENCY FACTOR OF PILE GROUP

In this section, the dynamic impedance of a 2 × 2 pile group is calculated through Equation (43). In order to directly reflect the influences of pile-to-pile interaction, the dynamic impedance of pile group k_G is divided by the sum of the static impedances of the individual single piles for producing group efficiency factor χ_G, which is written as:

$$\chi_G = \frac{k_G}{MM \times K_d^{\text{static}}(0)} \tag{45}$$

If the dynamic interaction between piles is not considered, the value ofχ_G should equals 1. Generally, for the static condition, $\chi_G$is always smaller than 1, which indicates that pile-to-pile interaction suppresses the dynamic impedance of pile group. For the dynamic condition, the value ofχ_G will varies with frequency. χ_G will exceed the value of 1 at certain frequencies, which indicates that dynamic impedance of the pile group is greater than that of the sum of the static impedances of individual piles.

6.1 | Effects of subsoil layer stiffness

Figures 17, 18, and 19 show the fluctuation of group efficiency factor χ_G against frequency for the 2 × 2 fully embedded pile group on the subsoil layers with various stiffness. It is observed that greater subsoil stiffness brings greater group efficiency factor at the given frequency range of $a_0 < 1$ in Figure 17A, which is because that improving subsoil stiffness can significantly increase the dynamic impedance of pile group k_G. The real part ofχ_G for $E_{s2} = 40E_{s1}$ is around three times of that for $E_{s2} = E_{s1}$ at static condition. When the ratio of E_{s1}:E_{s2} is larger than 0.25, χ_G gradually decreases as frequency increases while χ_G shows a slowly increasing trend when E_{s1}:E_{s2} is smaller than 0.05. That different trend amplifies the effects of subsoil layer stiffness on the real part ofχ_G. Figure 17B shows that the imaginary part of χ_G increases with

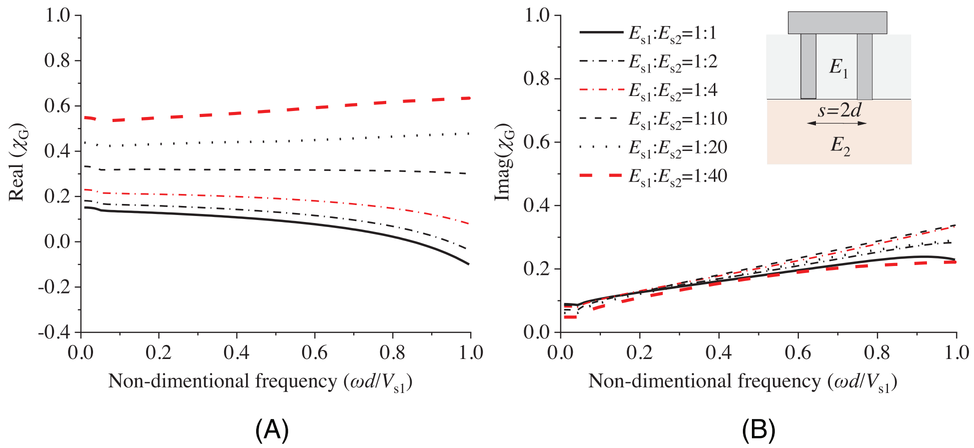

FIGURE 17 Group efficiency factors for the fully embedded pile group with s = 2d on various subsoil layers. L = 15d; H_0 = 0; E_p = 1000E_{s1}; ρ_p:ρ_{s1}:ρ_{s2} = 1.33:1:1; $\kappa_1 = \kappa_2$. (A) Real part, (B) Imaginary part.

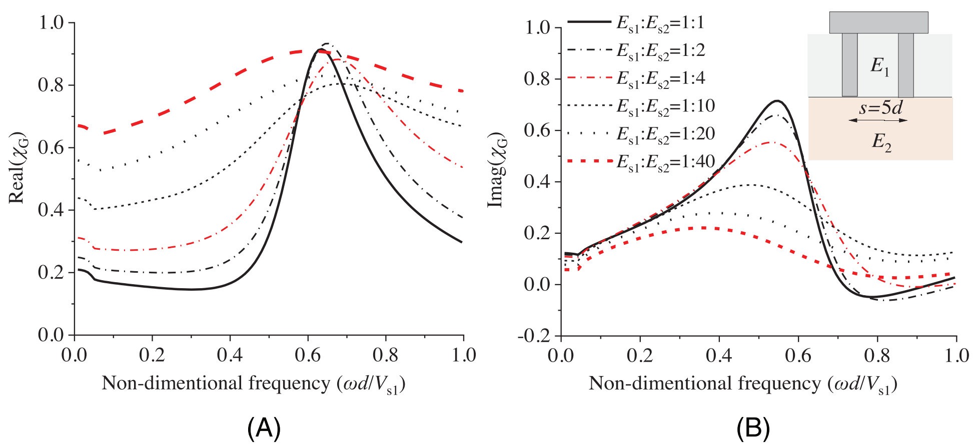

FIGURE 18 Group efficiency factors for the pile group with s = 5d on various subsoil layers. L = 15d; H_0 = 0; E_p = 1000E_{s1}; ρ_p:ρ_{s1}: ρ_{s2} = 1.33:1:1; $\kappa_1 = \kappa_2$. (A) Real part. (B) Imaginary part.

frequency. In contrast to the real part ofχ_G, the results of imaginary parts for various subsoil stiffness do not behave prominent difference when pile spacing s equals two times of pile diameter.

Both real part and imaginary part results of group efficiency factor for s = 5d in Figure 18 show obvious fluctuation with frequency. In Figure 18A, it is observed that the real parts of χ_G for various subsoil stiffness increase to their peaks at a narrow range of frequency from a_0 = 0.6 to 0.7. The difference of χ_G for various subsoil stiffness initially grows at $0 < a_0 < 0.4$ and then dramatically falls until χ_G comes to its peak around a_0 = 0.7. After that, χ_G for various subsoil stiffness reduce with various speed rates as frequency grows and their real part difference increases again. Figure 18B shows that increasing the subsoil modulus leads to a more significant fluctuation for the imaginary part of χ_G, which just accounts for the sharper growth around the peaks of χ_G for the cases of greater subsoil modulus in Figure 18A.

When pile spacing s is 10 times of pile diameter, it is observed that the curves of real part against frequency for various subsoil stiffness are approximately parallel to each other in Figure 19A. Besides that, both the real and imaginary parts of χ_G in Figure 19 fluctuate faster but flatter with frequency compared with the results for s = 5d. It is also interesting to observe that increasing pile spacing generally increases the value of χ_G and thus improves the work efficiency of pile group.

6.2 | Effects of surface soil layer stiffness

Producing non-dimensional frequency requires shear velocity of soil. Various surface soil stiffnesses lead to various shear velocities, which causes inconveniences for demonstrating the variation of group efficiency factor χ_G using

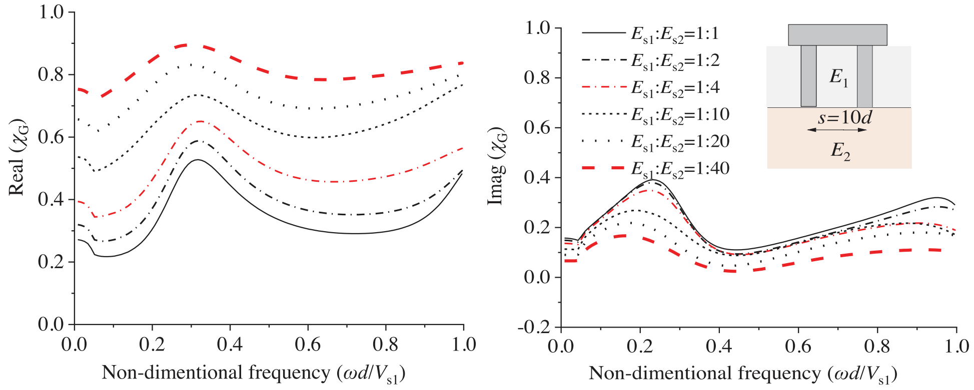

(A) (B)

FIGURE 19 Group efficiency factors for the pile group with $s = 10$d on various subsoil layers. $L = 15$d; $H_0 = 0$; $E_p = 1000E_{s1}$; ρ_p:ρ_{s1}: ρ_{s2} = 1.33:1:1; $\kappa_1 = \kappa_2$. (A) Real part. (B) Imaginary part.

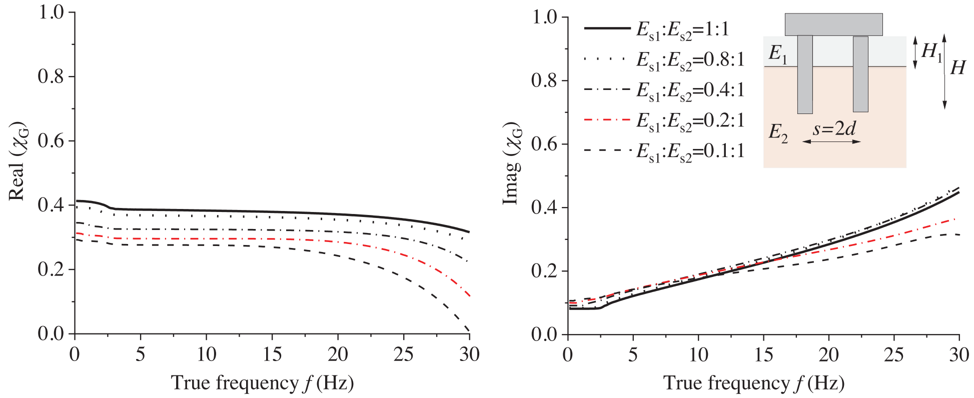

(A) (B)

FIGURE 20 Group efficiency factors of pile group for $s = 2$d in the surface soil layers of various stiffness. $L = 20$d; $H_1 = 5d$; $E_p = 100E_{s2}$; ρ_p:ρ_{s1}: ρ_{s2} = 1.33:1:1; $\kappa_1 = \kappa_2$. (A) Real part. (b) Imaginary part.

non-dimensional frequency. Thus, the true frequency is used for analysis from this section. Figures 20–22 depict the curves of group efficiency factor $\chi_G$against true frequency for the pile group in double-layered soil. The Young's modulus of the surface soil layer E_{s1} varies from 250 to 25 MPa and the thickness of the surface layer H_1 is a constant of 5d. It is observed in Figure 20A that the real part of χ_G has quite limited variation in 0-30 Hz when $E_{s1} = E_{s2} = 250$ MPa or E_{s1}:E_{s2} = 1:1. As E_{s1} decreases, the values of χ_G tend to reduce with frequency. That reduction is especially obvious in high-frequency range (greater than 15 Hz). When $E_{s1} = E_{s2} = 25$ MPa or E_{s1}:E_{s2} = 0.1:1, the real part of χ_G is close to zero at 30 Hz and the corresponding reduction is around 30% compared with the static case. The gradually increasing imaginary parts of χ_G in Figure 20B explain the reduction of real part at high frequencies for $s = 2$d.

The group efficiency factor for $s = 5$d in Figure 21A has its maximum at around 23 Hz when E_{s1}:E_{s2} = 1:1 and the corresponding peak value of χ_G is around two times (or 200%) of the static efficiency factor. By contrast, when E_{s1}:E_{s2} = 0.1:1, that increase of χ_G from static value to the peak value is only around 80%, which reflects that a reduction of surface soil stiffness could significantly impair the group efficiency factor. Similar results can be found in Figure 22 for $s = 10$d. It is also observed that the effects of surface soil layer stiffness on the imaginary parts of χ_G are less prominent than that on the real parts as shown in Figures 20B, 21B, and 22B.

Furthermore, Figures 23 and 24 depict the influences of the thickness of the surface weak soil on the group efficiency factor. The Young's modulus of the surface layer and the soil below it is 100 and 250 MPa, respectively. The thickness of surface weak soil varies from 2d to 10d. The results in Figure 23A show that increasing the thickness of surface weak soil could lead to a reduction for the real part of χ_G. When the thickness of the surface weak soil increases, both k_G and $K_d^{static}(0)$ decrease. Once the degree of decrease for k_G is larger than that for the $K_d^{static}(0)$, a reduction is observed for the

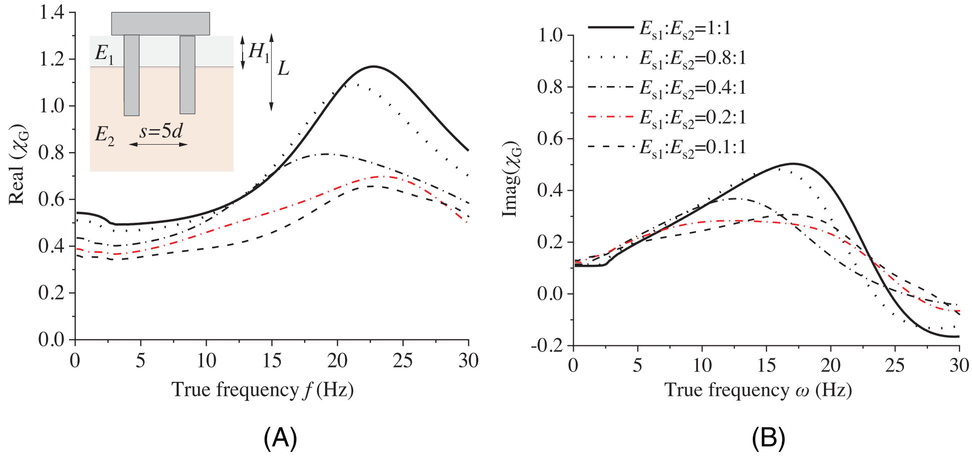

FIGURE 21 Group efficiency factors of pile group for s = 5d in the surface soil layers of various stiffness. L = 20d; H_1 = 5d; E_p = 100E_{s2}; ρ_p:ρ_{s1}:ρ_{s2} = 1.33:1:1; $\kappa_{1\,=}\,\kappa_2$. (A) Real part. (b) Imaginary part.

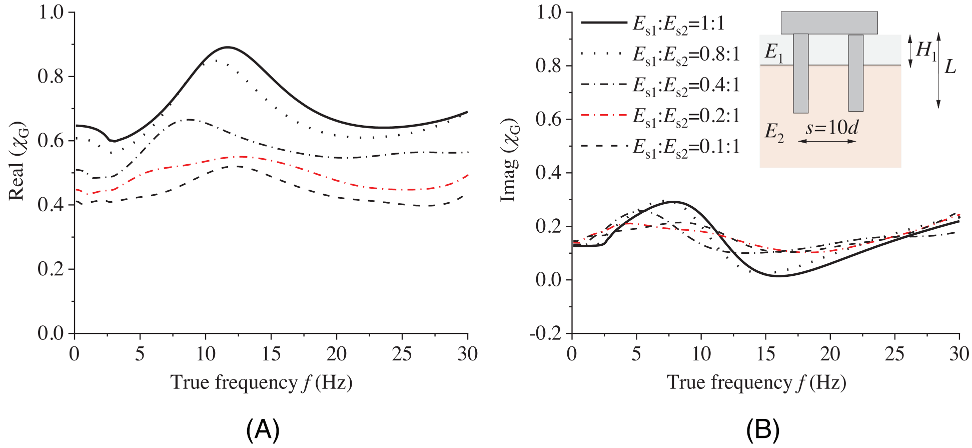

FIGURE 22 Group efficiency factors of pile group for s = 10d in the surface soil layers of various stiffness. L = 20d; H_1 = 5d; E_p = 100E_{s2}; ρ_p:ρ_{s1}:ρ_{s2} = 1.33:1:1; $\kappa_{1\,=}\,\kappa_2$. (A) Real part. (b) Imaginary part.

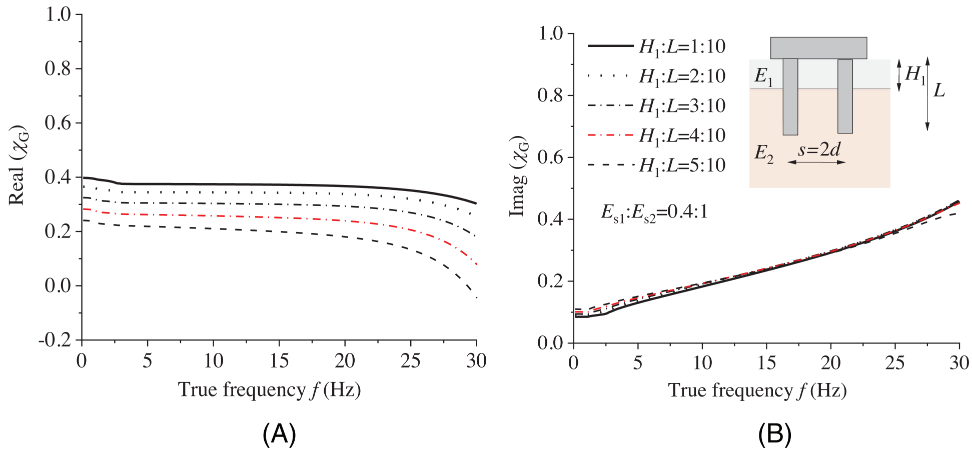

FIGURE 23 Group efficiency factors of pile group for s = 2d in the surface soil layers of various thickness. L = 20d; H_0 = 0; E_{s1}: E_{s2} = 2:5; E_p = 100E_{s2}; ρ_p:ρ_{s1}: ρ_{s2} = 1.33:1:1; $\kappa_{1\,=}\,\kappa_2$. (A) Real part. (B) Imaginary part.

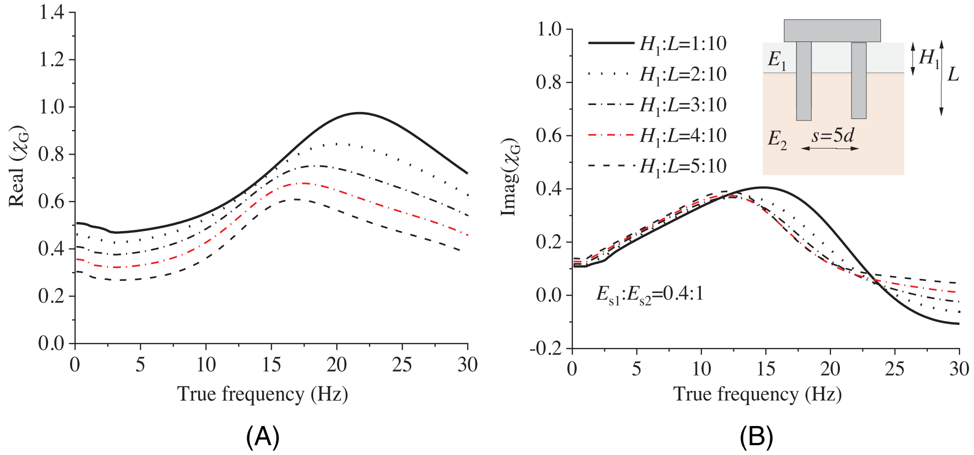

FIGURE 24 Group efficiency factors of pile group for s = 5d in the surface soil layers of various thickness. L = 20d; H_0 = 0; E_{s1}: E_{s2} = 2:5; E_p = 100E_{s2}; ρ_p:ρ_{s1}:ρ_{s2} = 1.33:1:1; $\kappa_1 = \kappa_2$. (A) Real part. (B) Imaginary part.

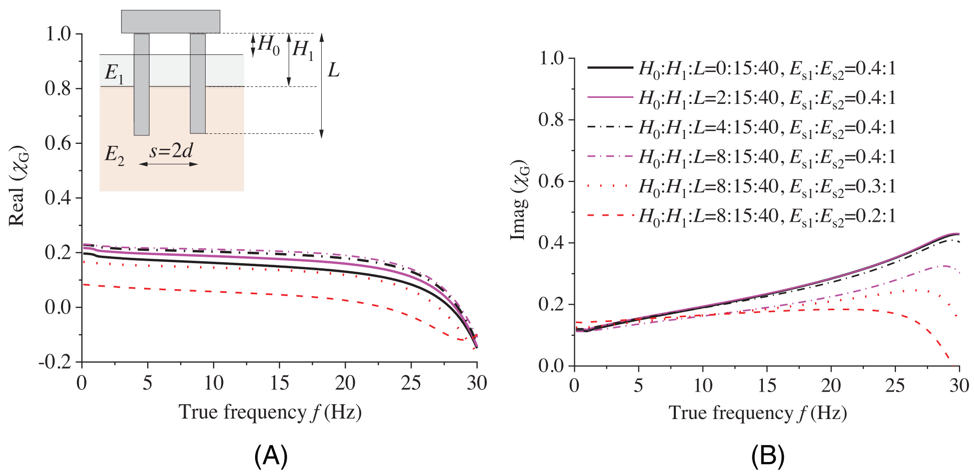

FIGURE 25 Group efficiency factors of the pile group with various unembedded segment lengths for s = 2d. L = 40d; E_p = 100E_{s2}; ρ_p:ρ_{s1}:ρ_{s2} = 1.33:1:1; $\kappa_1 = \kappa_2$. (A) Real part. (B) Imaginary part.

group efficiency. The results in Figure 23A indicate that increasing the thickness of the surface weak soil leads to more reduction for the dynamic impedance of pile group than that for the static impedance of single piles. When s = 2d, that reduction becomes significant when the excitation frequency exceeds 20 Hz. At the same time, Figure 23B shows that the thickness variation of surface soil has quite small influence on the imaginary part of χ_G, which indicates that thickness of surface soil layer could not cause obvious phase variation.

The results in Figure 24A for s = 5d predict that the peak values of real part of χ_G occur at the frequencies from 15 to 23 Hz and are around twice compared with their static impedances. Significant reduction of the real part of χ_G due to thickness growth is also observed in Figure 24A for s = 5d while the influence on the imaginary part of χ_G is overall small.

6.3 | Effects of unembedded segment length

Considering the extreme case that there is no soil around the pile, that is, unembedded segment length equals pile length, there will no soil–pile interaction happen and thus the group efficiency equals one. Figures 25 and 26 show the effects of unembedded segment length (H_0) on the group efficiency factor for s = 2d and s = 5d, respectively. It is observed in

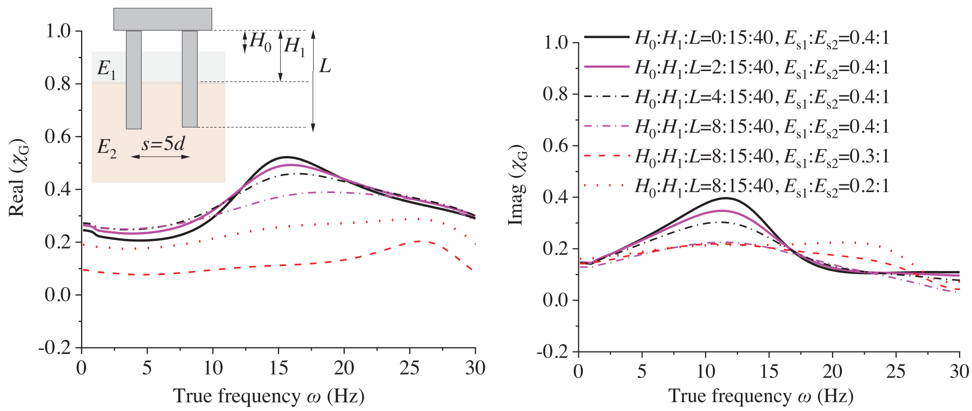

FIGURE 26 Group efficiency factors of the pile group with various unembedded segment lengths for s = 5d. $L = 40d$; $E_p = 100E_{s2}$; ρ_p:ρ_{s1}:ρ_{s2} = 1.33:1:1; $\kappa_1 = \kappa_2$.

Figure 25A that the extension of unembedded pile segment can slightly increase the real part of χ_G. That increase from 0d to 8d varies with frequency and it comes to the maximum of around 46% at 20 Hz in given frequency range. Figure 25B shows that the imaginary part of χ_G decreases as the unembedded segment length grows, whereas that decrease is limited, and the level is only 28% even when $H_0 = 8d$ or 20% of the whole pile length. Moreover, it is interesting to note that χ_G in both Figure 25A,B will significantly fall if the stiffness of the surface soil layer is simultaneously reduced for the partially embedded pile group.

The results for s = 5d in Figure 26 show more obvious fluctuation of group efficiency factor against frequency compared with those for s = 2d. Increasing unembedded segment length does not always lead to growth or reduction for χ_G when s = 5d. Both the real part in Figure 26A and the imaginary part in Figure 26B show flatter variation with frequency as unembedded segment length increases. Besides that, the fall of χ_G due to reduction of surface soil stiffness is still prominent as shown in Figure 26A.

7 | CONCLUSIONS AND DISCUSSION

In conventional energy method for pile-soil system, soil attenuation factor is assumed to be depth-independent to exclusively focus on the responses of single piles, which limits the algorithm extension in dynamic domain from single pile to pile group. This study develops a theoretical model for the dynamic pile-to-pile interaction and group efficiency factor for the partially embedded pile group in layered soil by combining the energy method and numerical simulations. The present model comprises three steps: solving the dynamic impedance of single pile, obtaining the soil attenuation factor and the pile-to-pile interaction factor in layered soil, and calculating the dynamic impedance and the group efficiency factor of pile group. The soil attenuation factor from the present method considers the influences of pile geometric and pile–soil stiffness ratio. The pile-to-pile interaction factor from this present method is directly solved through matrix equations, which is quite convenient because it avoids the artificial separation of soil attenuation factor and diffraction function. The effects of subsoil stiffness, surface soil stiffness, and unembedded segment length on the group efficiency factor of pile group are examined. Based on the results, the following conclusions can be drawn:

a. In homogeneous soil, the presented energy method gives slightly smoother amplitudes of soil attenuation factor and dynamic interaction factor at low-frequency range than FEM while plane stain method overestimates the results. Besides that, energy method is capable to predict the effects of pile geometry and stiffness ratio of pile and soil on the soil attenuation factor.
b. In layered soil, the phase of waves in each soil layer greatly relies on its stiffness. The soil attenuation factors obtained by the proposed method can take the wave speed difference in various layers into account, especially for the phase difference. The dynamic interaction factor produced by this proposed method is slightly reduced at very low frequency range. From the engineering perspective, the non-linear deformation on the pile–soil interface will significantly impair pile-to-pile interaction. Thus, the overestimation of pile-to-pile interaction from plane method is not anticipated. This

present method could give an alternative option to find a suitable dynamic interaction factor at low frequency range than the plane strain method or FEM in linearly elastic regime.

c. The variation of pile spacing exerts limited influences on group efficiency factor of pile group at the static condition. The stiffness or real part of the group efficiency factor fluctuates faster but milder with frequency when pile spacing becomes larger. The obvious reduction at high frequency range may be unfavorable to the mechanical behavior of piles for s = 2d. For s = 5d or 10d, the value of group efficiency factor may be close to 1 or even exceeds 1 at some certain frequencies, which is beneficial to the mechanical performance.
d. The real part of group efficiency factor generally increases with greater subsoil stiffness, greater surface soil stiffness. That increase varies with frequency and sometimes may exceeds 100%. By the contrast, the abovementioned parameters play a less significant role on the imaginary part of group efficiency factor, especially for s = 2d and s = 10d. The variation of group efficiency factor against frequency becomes milder as unembedded segment length increases. The combined effects of longer unembedded segment and weaker surface soil will lead to prominent reduction to group efficiency factor in common frequency range.

ACKNOWLEDGEMENTS

This research was financially supported by the National Natural Science Foundation of China (No: 52208370); the Applied Basic Research Programs of Science and Technology Department in Sichuan Province, China (No: 2022NSFSC1086). We also appreciates the support and help from interdisciplinary innovation team of southwest Jiaotong university and responsible anonymous reviewers of this journal.

CONFLICT OF INTEREST STATEMENT

The authors declare no conflicts of interest.

DATA AVAILABILITY STATEMENT

The data that support the findings of this study are available from the corresponding author upon reasonable request.

ORCID

Liming Qu https://orcid.org/0000-0002-9240-8411
Xuanming Ding https://orcid.org/0000-0002-3563-2222

REFERENCES

1. Wu WB, Wang ZQ, Zhang YP, et al. Semi-analytical solution for negative skin friction development on deep foundations in coastal reclamation areas. *Int J Mech Sci*. 2023;62:521.
2. Peng Y, Liu HL, Li C, et al. The detailed particle breakage around the pile in coral sand. *Acta Geotech*. 2021;35(6):563-575.
3. Yuan BX, Li ZH, Zhao ZQ, et al. Experimental study of displacement field of layered soils surrounding laterally loaded pile based on transparent soil. *J Soils Sediments*. 2021;24:e1937. doi:10.1007/s11368-021-03004-y
4. Zhang C, Wu CW, Wang PG. Seismic fragility analysis of bridge group pile foundations considering fluid-pile-soil interaction. *Shock Vib*. 2020;40:1321. doi:10.1155/2020/8838813
5. Chen JB, Gilbert RB, Choo YS, et al. Two-dimensional lower bound analysis of offshore pile foundation systems. *Int J Numer Anal Methods Geomech*. 2015;42(9):516-541.
6. Militano G, Rajapakse R. Dynamic response of a pile in a multi-layered soil to transient torsional and axial loading. *Geotechnique*. 1999;49:91-109.
7. Connolly D, Galvín P, Olivier B, Romero A, Kouroussis G. A 2.5 D time-frequency domain model for railway induced soil-building vibration due to railway defects. *Soil Dyn Earthquake Eng*. 2019;120:332-344.
8. Chatterjee K, Choudhury D. Influence of seismic motions on behavior of piles in liquefied soils. *Int J Numer Anal Methods Geomech*. 2018;132(3):516-541.
9. Ghasemzadeh H, Alibeikloo M. Pile–soil–pile interaction in pile groups with batter piles under dynamic loads. *Soil Dyn Earthquake Eng*. 2011;72:998-1015.
10. Liang FY, Liang X, Hao Z, et al. Seismic response from centrifuge model tests of a scoured bridge with a pile-group foundation. *J Bridge Eng*. 2020;38(8):557.
11. Xu B, Wei K, Qin SQ. Experimental study of wave loads on elevated pile cap of pile group foundation for sea-crossing bridges. *Ocean Eng*. 2020;20:115. doi:10.1016/j.oceaneng.2019.106896
12. Zhang YP, Liu H, Wu WB, et al. A 3D analytical model for distributed low strain test and parallel seismic test of pipe piles. *Ocean Eng*. 2021;12:239.

13. Prendergast LJ, Gavin K, Doherty P. An investigation into the effect of scour on the natural frequency of an offshore wind turbine. *Ocean Eng*. 2015;31(1):1159-1170.
14. Prendergast LJ, Hester D, Gavin K. Development of a vehicle-bridge-soil dynamic interaction model for scour damage modelling. *Shock Vib*. 2016;111:31-40. doi:10.1155/2016/7871089
15. Bao T, Liu Z. Vibration-based bridge scour detection: a review. *Struct Health Monit*. 2017;155:105184. doi:10.1002/stc.1937
16. Ciancimino A, Jones L, Lampros S, et al. Experimental assessment of the performance of a bridge pier subjected to flood-induced foundation scour. *Géotechnique*. 2021;20:1-18. doi:10.1680/jgeot.20.P.230
17. Micu EA, Khan MA, Bhowmik B, et al. Scour repair of bridges through vibration monitoring and related challenges. *Proceedings of the 1st Conference of the European Association on Quality Control of Bridges and Structures*; 2022: 499-450. doi:10.1007/978-3-030-91877-4_57
18. Mylonakis G, Gazetas G. Vertical vibration and additional distress of grouped piles in layered soil. *Soils Found*. 1998;70:432-447.
19. Basu D, Prezzi M, Salgado R, Chakraborty T. Settlement analysis of piles with rectangular cross sections in multi-layered soils. *Comput Geotech*. 2008;39:131-143.
20. Shadlou M, Bhattacharya S. Dynamic stiffness of pile in a layered continuum. *Geotechnique*. 2014;25(4):303-319.
21. Kanellopoulos K, Gazetas G. Vertical static and dynamic pile-to-pile interaction in non-linear soil. *Géotechnique*. 2020;43(2):1784-1793.
22. Gazetas G, Makris N. Dynamic pile-soil-pile interaction. Part I: analysis of axial vibration. *Earthq Eng Struct Dyn*. 1991;220:115-132.
23. Cai YY, Liu ZH, Li TB, et al. Vertical dynamic response of a pile embedded in radially inhomogeneous soil based on fictitious soil pile model. *Soil Dyn Earthquake Eng*. 2020;38:1.
24. Qu LM, Ding XM, Kouroussis G, et al. Dynamic interaction of soil and end-bearing piles in sloping ground: numerical simulation and analytical solution. *Comput Geotech*. 2021a;49:91.
25. Novak M, Aboulella F, Nogami T. Dynamic soil reactions for plane strain case. *J Eng Mech-ASCE*. 1978;83:769-782.
26. Wang N, Wang KH, Wu WB. Analytical model of vertical vibrations in piles for different tip boundary conditions: parametric study and applicationsx. *J Zhejiang Univ Sci*. 2013;17:79-93.
27. Tian X, Hu W, Gong X. Longitudinal dynamic response of pile foundation in a nonuniform initial strain field. *KSCE J Civ Eng*. 2015;18:1656-1666.
28. Guan WJ, Jiang GS, Liu X, et al. Non-axisymmetric analysis of the vertical dynamic response of large-diameter pile in layered soil. *Comput Geotech*. 2023;155:105184.
29. Zheng CJ, Ding XM, Li P, Fu Q. Vertical impedance of an end-bearing pile in viscoelastic soil. *Int J Numer Anal Methods Geomech*. 2015;39:676-684.
30. Luan LB, Zheng CJ, Kouretzis G, Cao G, et al. Development of a three-dimensional soil model for the dynamic analysis of end-bearing pile groups subjected to vertical loads. *Int J Numer Anal Methods Geomech*. 2019;101:1-11.
31. Maeso O, Aznárez JJ, Garcıá F. Dynamic impedances of piles and groups of piles in saturated soils. *Comput Struct*. 2005;83:769-782.
32. Ma JJ, Liu FJ, Gao XJ, et al. Buckling and free vibration of a single pile considering the effect of soil–structure interaction. *Int J Struct Stab Dyn*. 2018;16(4):1971.
33. Li LC, Wu WB, Liu H, Lehane B. DEM analysis of the plugging effect of open-ended pile during the installation process. *Ocean Eng*. 2021;220:749.
34. Peng Y, Yin ZY, Ding XM. Analysis of particle corner-breakage effect on pile penetration in coral sand: model tests and DEM simulations. *Can Geotech J*. 2022;134:103917. doi:10.1139/cgj-2022-0038
35. Wang LH. Dynamic response of pile group in two-layered soils under scour condition by FEM-ALEM approach. *Appl Math Modell*. 2022;16:3339-3353.
36. Kouroussis G, Anastasopoulos I, Gazetas G, et al. Three-dimensional Finite Element Modelling of Dynamic Pile-Soil-Pile Interaction in Time Domain: *Proceedings of 4th ECCOMAS Thematic Conference*. National Technical University of Athens, Kos Island, Greece; 2013.
37. Messioud S, Sbartai B, Dias D. Estimation of dynamic impedance of the soil–pile–slab and soil–pile–mattress–slab systems. *Int J Struct Stab Dyn*. 2017;135(6):420.
38. Wu WB, Zhang YP. A review of pile foundations in viscoelastic medium: dynamic analysis and wave propagation modeling. *Energies*. 2022;37:423.
39. Zheng CJ, Gan SS, Luan LB, et al. Vertical dynamic response of a pile embedded in a poroelastic soil layer overlying rigid base. *Acta Geotech*. 2021;64(3):303-319.
40. Anoyatis G, Mylonakis G. Dynamic winkler modulus for axially loaded piles. *Geotechnique*. 2012;40:185-206.
41. Cui CY, Meng K, Wu YJ, et al. Dynamic response of pipe pile embedded in layered visco-elastic media with radial inhomogeneity under vertical excitation. *Geomech Eng*. 2018;109:209.
42. Gupta BK, Basu D. Dynamic analysis of axially loaded end-bearing pile in a homogeneous viscoelastic soil. *Soil Dyn Earthquake Eng*. 2018;19:1656-1666.
43. Zhang SP, Cui CY, Yang G. Vertical dynamic impedance of pile groups partially embedded in multilayered transversely isotropic saturated soils. *Soil Dyn Earthquake Eng*. 2019;14:79-93.
44. Shan Y, Ma WJ, Xiang K, et al. Vertical dynamic response of a floating pile in unsaturated poroelastic media based on the fictitious unsaturated soil pile model. *Appl Math Modell*. 2022;112:341-357.
45. Zheng CJ, Kouretzis G, Ding XM, Luan LB. Vertical vibration of end-bearing single piles in poroelastic soil considering three-dimensional soil and pile wave effects. *Comput Geotech*. 2022;197:106896.

46. Qu LM, Yang CW, Ding XM, et al. A continuum-based model on axial pile-head dynamic impedance in inhomogeneous soil. *Acta Geotech*. 2021b;39:676-684.
47. Qu LM, Yang CW, Ding XM, et al. Vertical vibration of piles with square cross-section. *Int J Numer Anal Methods Geomech*. 2021;45(18):2629-2653. doi:10.1002/nag.3280
48. Lee KM, Xiao ZR. A new analytical model for settlement analysis of a single pile in multi-layered soil. *Soils Found*. 1999;117(5):106-115.
49. Seo H, Basu D, Prezzi M, Salgado R. Load-settlement response of rectangular and circular piles in multilayered soil. *J Geotech Geoenviron Eng*. 2009;16(3):977-983.
50. Salgado R, Seo HY, Prezzi M. Variational elastic solution for axially loaded piles in multilayered soil. *Int J Numer Anal Methods Geomech*. 2013;146:423-440.
51. Dobry R, Gazetas G. Simple method for dynamic stiffness and damping of floating pile groups. *Géotechnique*. 1988;225(4):557-574.
52. Saitoh M, Padrón LA, Aznárez JJ, Maeso O, et al. Expanded superposition method for impedance functions of inclined-pile groups. *Int J Numer Anal Methods Geomech*. 2016;40:185-206.
53. Kouroussis G, Verlinden O, Conti C. Ground propagation of vibrations from railway vehicles using a finite/infinite-element model of the soil. *Proc IME, Part F: J Rail Rapid Transit*. 2009;241(4):405-413.
54. Gazetas G, Fan K, Kaynia A. Dynamic response of pile groups with different configurations. *Soil Dyn Earthquake Eng*. 1993;15:239-257.
55. Kouroussis G, Zhu S, Vogiatzis K. Noise and vibration from transportation. *J Zhejiang Univ Sci A*. (2021);22:1-5. https://doi.org/10.1631/jzus.A20NVT01

How to cite this article: Qu L, Kouroussis G, Lian J, Ding X. Vertical dynamic interaction and group efficiency factor for floating pile group in layered soil. *Int J Numer Anal Methods Geomech*. 2023;47:1953–1978.
https://doi.org/10.1002/nag.3546